Southern Plains Transportation Center
CYCLE 1

FINAL REPORT

2023–2024

USDOT BIL Regional UTC
Region 6

Internal Curing of 3D Printed Engineered Cementitious Composites: Paving the Way for Durable Infrastructure in the Southwest

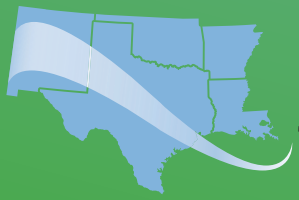

SOUTHERN PLAINS
TRANSPORTATION CENTER

Disclaimer

The contents of this report reflect the views of the authors, who are responsible for the facts and accuracy of the information presented herein. This document is disseminated under the sponsorship of the Department of Transportation University Transportation Centers Program, in the interest of information exchange. The U.S. Government assumes no liability for the contents or use thereof.

Technical Report Documentation Page

1. Report No. CY1-UNM-02	**2. Government Accession No.** [Leave blank]	**3. Recipient's Catalog No.** [Leave blank]
4. Title and Subtitle Internal Curing of 3D Printed Engineered Cementitious Composites: Paving the Way for Durable Infrastructure in the Southwest		**5. Report Date** January 15, 2025
		6. Performing Organization Code [Code]
7. Author(s) PI: Maryam Hojati, ORCID – 0000-0001-6043-7173, https://orcid.org/0000-0001-6043-7173 PhD Student: Tayyab Zafar https://orcid.org/0000-0002-8717-0453		**8. Performing Organization Report No.** [Report No.]
9. Performing Organization Name and Address University of New Mexico The University of New Mexico: Albuquerque, NM, USA		**10. Work Unit No. (TRAIS)** [Leave blank]
		11. Contract or Grant No. 69A3552348306
12. Sponsoring Agency Name and Address Southern Plains Transportation Center 202 West Boyd St., Room 213B The University of Oklahoma Norman, OK 73019		**13. Type of Report and Period Covered** Final Report (Oct 2023- Jan 2025)
		14. Sponsoring Agency Code [Leave blank]

15. Supplementary Notes
Conducted in cooperation with the U.S. Department of Transportation as a part of the University Transportation Center (UTC) program.

16. Abstract
This study investigated the feasibility of internal curing using lightweight aggregates (LWA) for 3D-printed engineered cementitious composites (ECC) on a small scale to advance durable infrastructure construction for future transportation needs. River sand (RS) was partially replaced with 30% natural pumice (NM) for internal curing, while cement was replaced with 50% slag, which is a byproduct of steel production. Polyethylene (PE) fibers were incorporated at 2% by volume to improve mechanical performance. The lightweight aggregates were presoaked for 24 hours before mixing to evaluate their effects on extrudability, buildability, and mechanical properties. Two mixes, S50-CT (control) and S50-P30 (pumice-modified), were 3D-printed and cured under varying relative humidity conditions before testing at 28 days. Including slag, methylcellulose (MC), and PE fibers reduced extrudability but improved the mechanical performance of the printed specimens. S50-CT demonstrated higher buildability, while S50-P30 exhibited superior compressive and flexural strength, highlighting the effectiveness of internal curing mechanisms. These mechanisms ensured sustained hydration, improved microstructural integrity, and enhanced crack resistance, resulting in greater durability. This study underscores the potential of internal curing with LWA and novel 3D printing techniques to achieve high-performance ECC materials for future infrastructure applications.

17. Key Words Engineered Cementitious Composites, 3-D Printing, Internal Curing, Supplementary Cementitious Materials, Fresh Properties, Hardened Properties, Lightweight Aggregates	**18. Distribution Statement** No restrictions. This publication is available at www.sptc.org and from the NTIS.		
19. Security Classification (of this report) Unclassified	**20. Security Classification (of this page)** Unclassified	**21. No. of Pages** 51 pages	**22. Price** N/A

Form DOT F 1700.7 (8-72) Reproduction of completed page authorized

INTERNAL CURING OF 3D PRINTED ENGINEERED CEMENTITIOUS COMPOSITES: PAVING THE WAY FOR DURABLE INFRASTRUCTURE IN THE SOUTHWEST

FINAL REPORT
SPTC Project Number: CY1-UNM-02

Submitted by
Dr. Maryam Hojati (PI)
Tayyab Zafar (Graduate Student)
Gerald May department of Civil, Construction, and Environmental Engineering
University of New Mexico

Prepared for
Southern Plains Transportation Center
The University of Oklahoma
Norman, OK

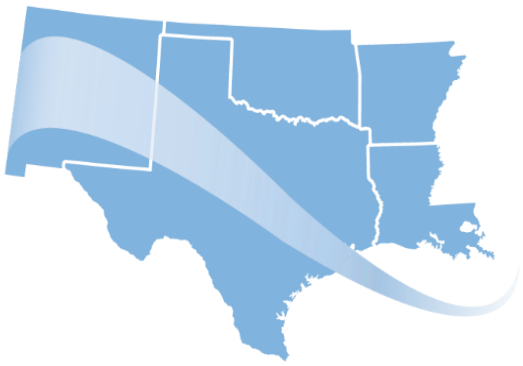

SOUTHERN PLAINS
TRANSPORTATION CENTER

January 2025

Acknowledgments

The authors gratefully acknowledge the financial support from SPTC under Award # CY1-UNM-R2.2. Any opinions, findings, conclusions or recommendations expressed in this material are those of the authors and do not reflect the views of SPTC. The authors would like to thank the invaluable assistance of Ms. Hamideh Shojaeian in laboratory work. All tests were performed in the Dana C. Wood Materials and Structures Lab at UNM. Additionally, the authors are grateful for supplying the required materials from GCC Cement and CR Minerals, which donated their material to this research. Furthermore, this document was reviewed and edited using ChatGPT to ensure clarity, grammatical accuracy, and coherence.

Table of Contents

List of Tables

List of Figures

List of Equations

List of Abbreviations and Acronyms

AM	Additive Manufacturing
ECC	Engineered Cementitious Composites
3D	Three Dimensional
3DPC	Three-Dimensional Printed Concrete
C	Cement
S	Slag
W	Water
RS	River Sand
B	Binder
HRWR	High Range Water Reducer
MC	Methyl Cellulose
PE	Polyethylene
NM Pumice	New Mexico Pumice
FRC	Fiber Reinforced Concrete
HSC	High Strength Concrete
UHPC	Ultra High Performance Concrete
SHCC	Strain Hardening Cementitious Composites
RH	Relative Humidity
LWA	Lightweight Aggregates
SAP	Super Absorbent Polymer

SI Conversion Factors

SI* (MODERN METRIC) CONVERSION FACTORS

APPROXIMATE CONVERSIONS TO SI UNITS

Symbol	When You Know	Multiply By	To Find	Symbol
		LENGTH		
in	inches	25.4	millimeters	mm
ft	feet	0.305	meters	m
yd	yards	0.914	meters	m
mi	miles	1.61	kilometers	km
		AREA		
in^2	square inches	645.2	square millimeters	mm^2
ft^2	square feet	0.093	square meters	m^2
yd^2	square yard	0.836	square meters	m^2
ac	acres	0.405	hectares	ha
mi^2	square miles	2.59	square kilometers	km^2
		VOLUME		
fl oz	fluid ounces	29.57	milliliters	mL
gal	gallons	3.785	liters	L
ft^3	cubic feet	0.028	cubic meters	m^3
yd^3	cubic yards	0.765	cubic meters	m^3
		NOTE: volumes greater than 1000 L shall be shown in m^3		
		MASS		
oz	ounces	28.35	grams	g
lb	pounds	0.454	kilograms	kg
T	short tons (2000 lb)	0.907	megagrams (or "metric ton")	Mg (or "t")
		TEMPERATURE (exact degrees)		
°F	Fahrenheit	5 (F-32)/9 or (F-32)/1.8	Celsius	°C
		ILLUMINATION		
fc	foot-candles	10.76	lux	lx
fl	foot-Lamberts	3.426	$candela/m^2$	cd/m^2
		FORCE and PRESSURE or STRESS		
lbf	poundforce	4.45	newtons	N
lbf/in^2	poundforce per square inch	6.89	kilopascals	kPa

APPROXIMATE CONVERSIONS FROM SI UNITS

Symbol	When You Know	Multiply By	To Find	Symbol
		LENGTH		
mm	millimeters	0.039	inches	in
m	meters	3.28	feet	ft
m	meters	1.09	yards	yd
km	kilometers	0.621	miles	mi
		AREA		
mm^2	square millimeters	0.0016	square inches	in^2
m^2	square meters	10.764	square feet	ft^2
m^2	square meters	1.195	square yards	yd^2
ha	hectares	2.47	acres	ac
km^2	square kilometers	0.386	square miles	mi^2
		VOLUME		
mL	milliliters	0.034	fluid ounces	fl oz
L	liters	0.264	gallons	gal
m^3	cubic meters	35.314	cubic feet	ft^3
m^3	cubic meters	1.307	cubic yards	yd^3
		MASS		
g	grams	0.035	ounces	oz
kg	kilograms	2.202	pounds	lb
Mg (or "t")	megagrams (or "metric ton")	1.103	short tons (2000 lb)	T
		TEMPERATURE (exact degrees)		
°C	Celsius	1.8C+32	Fahrenheit	°F
		ILLUMINATION		
lx	lux	0.0929	foot-candles	fc
cd/m^2	$candela/m^2$	0.2919	foot-Lamberts	fl
		FORCE and PRESSURE or STRESS		
N	newtons	0.225	poundforce	lbf
kPa	kilopascals	0.145	poundforce per square inch	lbf/in^2

Executive Summary

Additive Manufacturing (AM), or 3D printing, is revolutionizing industries by enabling flexible and efficient production processes. In engineering and architecture, it facilitates the rapid and economical creation of complex designs, offering transformative potential for infrastructure development. Engineered Cementitious Composites (ECC), known for their high ductility, crack control, and strain-hardening behavior, emerge as promising material for 3D printing civil infrastructure. Fiber-reinforced ECC, in particular, enhances structural capacity, durability, and resilience.

However, the exposure of 3D-printed ECC elements to ambient environmental conditions poses significant challenges, especially in arid regions like New Mexico. Low humidity can hinder hydration, weaken mechanical properties, and reduce durability. To address these challenges, this study investigates the feasibility of internal curing using lightweight aggregates (LWA) in 3D-printed ECC to ensure proper hydration and moisture distribution, thereby enhancing mechanical performance and crack resistance. Two ECC mixes were developed: a control mix (S50-CT) and a pumice-modified mix (S50-P30). River sand was partially replaced with 30% natural pumice for internal curing, while cement was replaced with 50% slag, which is a byproduct of steel production. Polyethylene (PE) fibers were incorporated at 2% by volume to improve ductility. The LWAs were presoaked for 24 hours to optimize their moisture content. Specimens were 3D-printed and subjected to curing under different relative humidity conditions, with mechanical performance tested at 28 days.

Flowability results indicated that the inclusion of slag, methylcellulose, and PE fibers reduced flowability, which enhanced the demand for water content; initially, a W/B ratio of 0.27 was selected, which was increased to 0.31 to achieve the required flow. An extrudability test was performed on the zigzag pattern to evaluate the printed filament's printing quality and shape retention. Results indicated that the inclusion of PE fibers at 2% volume reduced the printing quality but increased the shape retention of the printed filament, and the width of the printed filament was close to the designed width of the filament. Buildability test results showed that S50-CT had 18 layers stacked compared to S50-P30, which had 16. This can be attributed to the absence of presoaked lightweight aggregates. In contrast, in S50-P30, the moisture content is higher due to the presence of presoaked lightweight aggregates, which reduced the static yield stress and ultimately reduced the buildability. In low relative humidity, both the mixes showed a reduction in compressive strength, highlighting the effect of environmental conditions on the curing and hydration. S50-P30 showed promising mechanical results at lower relative humidity than the controlled specimen, confirming the presence of internal curing mechanisms, preventing moisture loss and ensuring continuous hydration under dry environmental conditions. S50-P30 at RH-75% demonstrated better compression strength results than S50-CT at RH-100%, which also complements the internal curing process in a dry environment. In terms of flexural strength, both the mixes showed a similar initial linear elastic response, even though the peak load for both the mixes is comparable, suggesting that both mixes have the same flexural capacity before significant cracking occurs. After the post-peak, S50-CT drops the load sharply, followed by smaller peaks exhibiting brittle behavior, poor crack bridging capacity, reduced ductility, and limited energy absorption. In the case of S50-P30, the post-peak load drops gradually and shows a smoother curve. This indicates that crack bridging capability has improved, and energy dissipation has increased. S50-P30 sustained larger deformations than S50-CT due to the enhanced internal curing, which improved its microstructure integrity, ductility, resistance to the crack, and toughness. S50-P30 demonstrated superior compressive and flexural strength compared to S50-CT, showcasing the effectiveness of internal curing

mechanisms in maintaining hydration and increasing durability. S50-CT showed higher buildability but lacked the mechanical benefits provided by internal curing.

This study underscores the potential of internal curing with lightweight aggregates to overcome hydration challenges in 3D-printed ECC. By advancing novel 3D printing technologies and durable material solutions, this research lays the groundwork for constructing durable, high-performance infrastructure in arid regions, contributing to the future of transportation construction.

Chapter 1. Introduction

Additive Manufacturing (AM), commonly known as 3D printing, has been hailed as the next industrial revolution due to its potential for flexible and efficient production of industrial products. In the context of engineering and architecture, 3D printing allows for the economical and rapid creation of complex representational models during the design phase. Engineered Cementitious Composites (ECC) emerge as a promising material for 3D printing infrastructure, showcasing high ductility, narrow crack width, and a unique strain-hardening behavior akin to metals. ECC's implementation, particularly the fiber-reinforced variant, is expected to enhance structural capacity, durability, and resilience in 3D-printed civil infrastructure.

However, the exposure of 3D-printed elements to the ambient environment poses a challenge, potentially leading to improper hydration and weaker materials, especially in low-humidity regions like New Mexico. To address this concern, this project explored internal curing to ensure proper hydration and moisture distribution within the concrete, thereby improving durability and reducing cracking.

Problem Statement

The primary issue addressed in this project is the potential weakening of 3D-printed ECC structures due to inadequate hydration caused by exposure to the ambient environment, especially in dry regions like New Mexico. The project recognized this challenge and aimed to investigate the feasibility of using internal curing to enhance the durability of 3D-printed ECC materials on a small scale. The ultimate goal is to adapt novel 3D printing technology for the future of transportation construction, emphasizing enhanced mechanical performance in arid conditions.

Research Objectives

The research approach involves several technical objectives:

1. Advance innovative manufacturing techniques, including 3D printing, in transportation infrastructure projects in low-humid regions.
2. Modify ECC mixes developed by the PI team to enhance their mechanical and durability performance by incorporating internal curing agents, specifically lightweight aggregates. A 50% weight substitution of cement with suitable byproduct alternatives (slag) was implemented.
3. Investigate the effect of different types (local NM pumice) and contents of internal curing agent at 30% substitution for normal weight aggregates on the performance of ECC for transportation infrastructure.
4. Ensure printable ECC mixes performance by thoroughly examining fresh properties like water content, extrudability, and buildability for 3D printing by 3D printing a zigzag pattern and wall.
5. Assessing the feasibility of designing an ECC mix suitable for 3D printing infrastructure in arid conditions. This was achieved by evaluating mechanical properties, including compressive and flexural, across three distinct curing regimes. The goal is to establish an ECC composition demonstrating robust mechanical performance and durability within dry environments, enhancing its suitability for 3D-printed infrastructure applications.
6. Explore utilizing locally available NM pumice to enhance the economic viability of the 3D-printing process and the ECC used in transportation infrastructure projects.

Chapter 2. Literature Review

Engineered Cementitious Composites (ECC)

ECC falls within the broader category of fiber-reinforced concrete (FRC) (Zafar et al., 2023a), as it incorporates fibers within a cementitious matrix. When subjected to tensile loads, FRCs typically show tension-softening behavior, where cracks appear and progressively widen as the load resistance capacity diminishes. For both regular concrete and FRC, the elastic limit is typically approached at approximately 0.01%. A relatively more recent type of material, Ultra-High-Performance Concrete (UHPC), is characterized by optimized gradation of granular constituents, highlighting high compressive strength (exceeding 150 MPa) and the ability to maintain post-cracking tensile strength of 5 MPa. Generally, UHPC exhibits a tensile deformation capacity of 0.2% or less (Figure 1) (Biyani et al., 2020).

In contrast, The ECC material family is characterized by its ductility, with a tensile strain capacity that typically exceeds 2%. (Figure 1) (Li, 2003). The design philosophy behind ECC remarkably differs from that of high-strength concrete (HSC) or UHPC. While HSC and UHPC are designed based on dense packing of particles, ECC's material microstructure is intentionally adjusted to foster synergistic interactions among its microstructural components. This approach, called micromechanics of ECC, involves deliberately engineering the fiber, matrix, and fiber/matrix interaction in a specific manner when subjected to load. The emphasis on this design principle is the rationale behind its name, Engineered Cementitious Composites (Şahmaran et al., 2009).
The fundamental objective of ECC's design is to address a critical limitation present in traditional concrete, specifically its limited capacity for tensile deformation. Consequently, ECC shows a stress-strain relationship more reminiscent of metallic materials, featuring a distinct "yield" strength followed by tensile strain-hardening behavior. During this phase, the stress-strain relationship is represented by a straight line with a slope lower than the elastic modulus, marked by multiple load drops whose magnitude depends on the specific ECC variant. This characteristic has led to ECC being termed Strain-Hardening Cementitious Composites (SHCC), emphasizing its nearly bi-linear relationship between tensile stress and strain and its applicability in structural design (Li et al., 2020).

The tensile ductility of ECC, denoting its deformation capacity at peak strength, is typically two orders of magnitude greater than that of regular concrete. Its compressive strength varies, ranging from a few MPa, as seen in fire-resistant, highly insulative ECC designed for steel protection, to exceeding 200 MPa in ultra-high-strength ECC engineered for impact loading (Figure 1). illustrates the tensile stress-strain relationship for these two ECC types, showcasing their distinctive characteristics. The deformability and propensity for multiple cracking in ECC are depicted in Figure 2. ECC places a strong emphasis on tensile ductility with the goal of supporting infrastructure resilience and durability by mitigating fracture failures.

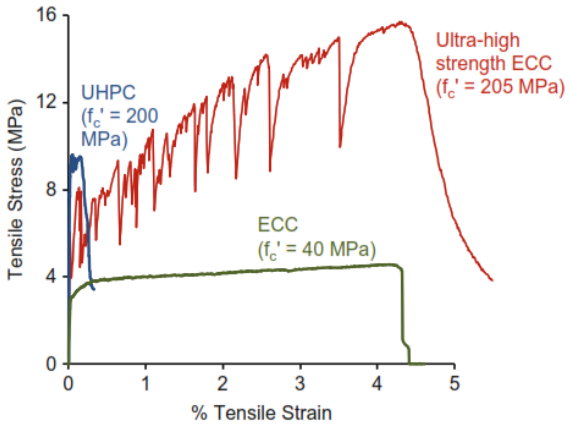

Figure 1. Tensile curves of Normal strength and High strength ECC and UHPC (Biyani et al., 2020)

Figure 2. High Deformability of ECC under a) bending load and b) direct tension (Biyani et al., 2020)

3D Printing of Engineered Cementitious Composites

Additive manufacturing, also known as 3D printing, according to the definition by ASTM Committee F42 (*ASTM Committee F42 on Additive Manufacturing Technologies*, 2009), involves the layer-by-layer fabrication of an object or component based on a 3D computer-aided design. Integrating innovative technologies like 3D printing has transformed the construction industry by enabling the direct creation of intricate and complex geometries through printing, eliminating the need for traditional formwork methods. Compared to conventional construction approaches, additive manufacturing presents several benefits, including expedited construction processes, reduced labor demands, safer working conditions, and minimized material waste (Sedghi et al., 2023).

Despite three decades of 3D printing technology in construction, various challenges remain to be addressed to fully unlock its potential in structural printing. Some of these highlighted limitations include modifying the properties of 3D printable cementitious materials through admixtures and additives, ensuring the durability of printed concrete, exploring 3D printing of fiber-reinforced concrete, and addressing the incorporation of reinforcement during the printing process (Robayo-Salazar et al., 2023).

A major challenge impeding the widespread acceptance of concrete 3D printing in civil infrastructure lies in the complexity of incorporating reinforcement into printed structural elements to ensure robust performance under various loading conditions. The conventional method of reinforcing materials is unsuitable for 3D-printed materials, necessitating essential material and reinforcement strategy modifications to make 3D printing a viable construction practice.

To reinforce 3D-printed cementitious materials, pre- and post-installation of prefabricated steel rebars and reinforcement is one approach. However, it restricts nozzle movement during printing and lacks full automation for the entire construction process. In contrast, incorporating fiber reinforcement into the fresh concrete mixture during printing is deemed more compatible and practical for 3D printing technology. Therefore, a self-reinforced ECC mixture with superior properties emerges as a novel candidate for 3D printing construction, aiming to enhance the ductility (softening) and tensile capacity (hardening) of 3DPC elements through the in-process reinforcement technique (Zafar et al., 2023a). However, adjustments in the fresh characteristics of the ECC mixture are necessary to meet the requirements for 3D printing.

Internal curing and 3D Printing of ECC

Concrete 3D printing represents an innovative formwork-free construction method wherein printable materials are extruded through a nozzle and stacked in successive layers. In comparison to conventional concrete casting, this technique offers significant advantages, including high automation, enhanced construction safety, and reductions in time, formwork, and labor costs (Wang et al., 2020). However, the absence of formwork protection exposes 3D-printed concrete (3DPC) to moisture loss both during the printing process and after deposition.

Environmental conditions, like hot climate, high wind speed and low relative humidity (RH), can intensify moisture evaporation from the surface of concrete during and after printing(Gerrit M. Moelich et al., 2020)(Li et al., 2020). The extensive exposed area of 3DPC facilitates the outward movement of internal moisture, hindering the hydration reaction of cement and resulting in insufficient hydration products to fill the pores. Consequently, the mechanical properties of 3DPC decline due to increased porosity and coarse pores (Ma et al., 2022).

Apart from water evaporation post-deposition, evaporation during printing also impacts the bond properties between consecutive layers (Chen et al., 2020). Moisture evaporation becomes more pronounced with longer time intervals between layers, reducing interlayer bond strength and overall mechanical properties of 3DPC (Van Der Putten et al., 2021). Studies have shown a significant decrease in interlayer bond strength (47.7%) with increased printing time intervals (Sanjayan et al., 2018).

The higher stiffness of the printed material, combined with prolonged printing intervals, introduces pores and flaws into the printed filaments (Nerella et al., 2019). Following deposition, the absence of formwork increases the exposed area, amplifying the adverse effects of ambient environmental conditions on the mechanical properties of the printed material (Soja et al., 2020).

Bendable concrete is different from traditional concrete as it has very low W/CM to satisfy ECC's micromechanics and interface properties. Increased W/CM reduces the concentration of binder particles, resulting in loose microstructure and weak interfacial bonding (Kong et al., 2003), which will result in low fiber bridging stress and low tensile capacity in terms of strength as well as strain. High W/CM also decreases the plastic viscosity of ECC, resulting in poor fiber

distribution. Therefore, because of the low W/CM (less than 0.30), one of the major challenges with bendable concrete is its tendency to undergo early-age cracking resulting from enhanced autogenous shrinkage that may affect the durability properties of the ECC (Şahmaran et al., 2009). Due to the dense microstructure of the ECC, water transportation is hindered from the surface to the core of the ECC; therefore, external curing methods are ineffective in eliminating early-age cracking (D. P. Bentz et al., 1999).

An effective way to control this issue is the use of pre-wetted lightweight aggregates (LWA) as internal curing water storage (H. K. Kim et al., 2018; Şahmaran et al., 2009). According to the American Concrete Institute (ACI), the definition of internal curing is "supplying water throughout a freshly placed cementitious mixture using reservoirs, via pre-wetted lightweight aggregates, that readily release water as needed for hydration or to replace moisture lost through evaporation or self-desiccation" (Jason Weiss, Dale Bentz, Anton Schindler, 2012). Figure 3 compares concrete's external and internal curing using presoaked lightweight aggregates (LWA) (J. Yang et al., 2024). To maintain the relative humidity in the matrix and alleviate the autogenous shrinkage, internal curing is considered the most effective technique (Liu et al., 2017; Mechtcherine et al., 2013; Schroefl et al., 2017; L. Yang et al., 2021).

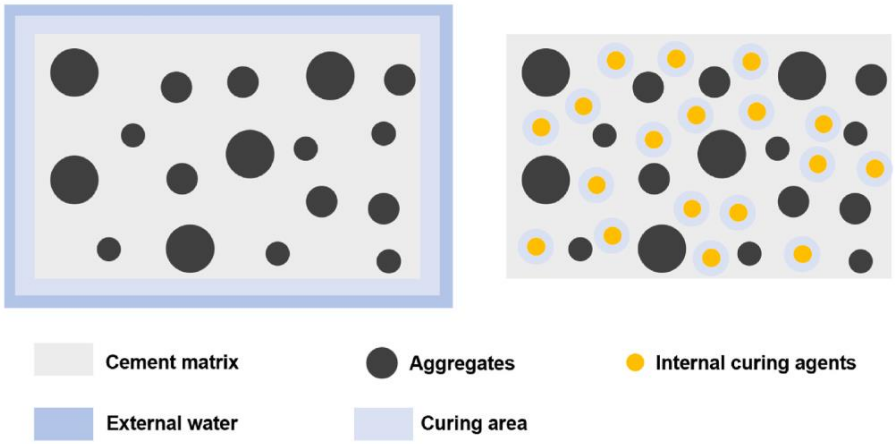

Figure 3. Conventional and Internal Curing of Concrete (J. Yang et al., 2024)

When the moisture inside the capillary pores is slowly consumed during the hydration process, resulting in increased capillary pressure and a drop in relative humidity, then water stored in the internal curing agent is released under the relative humidity gradient formed due to the difference of pore size of internal curing agent (larger pores) and capillary pores (smaller pores). Water transportation is also promoted due to the difference in capillary pressure between the internal curing agent and concrete matrix (L. Yang et al., 2021). By adding the internal curing agents, the meniscus radius can be increased, reducing the capillary pressure and reducing the driving force that causes shrinkage. The released water migration distance in the hardening concrete and the water absorption/desorption behavior of internal curing agents have significant effects on internal curing (D. P. Bentz et al., 1999; J. H. Kim et al., 2018; Semion Zhutovsky et al., 2004).

Internal curing agents are broadly classified into two categories based on their water absorption method. The first type of internal curing agent absorbs water through physical capillary forces, such as rice husk ash, zeolite, perlite, expanded shale, expanded glass, pumice and recycled aggregates, which are porous materials. Because of their low cost and easy availability, lightweight aggregates are the most common internal curing agents from the first type (Liu et al.,

2017). The second type of internal curing agents are superabsorbent polymers (SAPs), which can absorb and retain water up to a hundred times their self-weight. SAP's water absorption mechanism is through van der Waal forces or hydrogen bonds (J. Yang et al., 2024). When SAPs release retained water, that reduces capillary pressure, ultimately causing a reduction in plastic shrinkage and crack severity. Similarly, it increases internal relative humidity and causes a reduction in autogenous shrinkage during self-desiccation. The premature release of water from SAPs can result in a drop of mechanical strength because of increased W/C. However, In 3D printed concrete (3DPC), the inter layer bond strength can be enhanced by the increased surface moisture or by the reduction of differential shrinkage strain (G. M. Moelich et al., 2022)(Gerrit Marius Moelich et al., 2021). The buildability of 3DPC can be improved significantly through SAPs by absorbing free pore water after extrusion (Gerrit Marius Moelich et al., 2021).

Several studies have reported that replacing normal aggregates with presoaked lightweight aggregates as an internal curing agent has effectively mitigated autogenous shrinkage in high-performance concrete with low W/C (Şahmaran et al., 2009). In addition to the mitigation of autogenous shrinkage, internal curing can increase the rate of hydration, which may result in improved mechanical and durability properties of high-strength concrete. Several studies have reported that at later ages, the improved strength and resistance to chloride attack are attributed to the enhanced hydration caused by the internal curing from the lightweight aggregates (H. K. Kim et al., 2018). The effectiveness of internal curing agents in alleviating autogenous shrinkage depends on the higher water absorption capacity of LWA and the fineness of its particle size (S. Zhutovsky et al., 2002). Optimum efficiency of volcanic pumice LWA was observed in the range of 0.59 to 4.76 mm (Şahmaran et al., 2009).

In conclusion, the primary issue being addressed in this project is the potential weakening of 3D-printed ECC structures due to inadequate hydration caused by exposure to the ambient environment, especially in dry regions like New Mexico. Therefore, to overcome the issue of insufficient hydration and increase the overall durability of 3D-printed ECC materials, the research proposes the implementation of internal curing. Internal curing involves the introduction of lightweight aggregates, specifically utilizing locally available materials like NM Pumice as internal curing agents, which will facilitate sustained moisture distribution within the ECC during the curing process. This intervention is expected to improve the material properties of the 3D-printed ECC significantly, mitigating issues related to early-age cracking, reduced mechanical strength, and compromised durability.

Chapter 3. Materials and Methodologies

Materials

The mixture design of Engineered Cementitious Composites is adapted from the author's previous work. The constituents of the mix include Ordinary Portland Cement (C), mineral admixtures, chemical admixtures, River Sand, Lightweight Aggregates, and fibers. Ordinary Portland Cement (C) was provided by the GCC Cement in New Mexico, confirming the ASTM C150 standard for Type I/II. Table 1 displays the chemical compositions of the introduced binding materials. In addition to the binder components, methylcellulose was used as a rheology modifying agent and Polyethylene (PE) fiber was added to provide acceptable tensile capacity(Zafar et al., 2023b). The properties of these materials are reported in Table 2 and Table 3.

Table 1. Chemical composition of binders (C, S) and lightweight aggregate

Material	SiO_2	Al_2O_3	Fe_2O_3	CaO	MgO	SO_3	K_2O	TiO_2	Na_2O	Specific Gravity
C	19.24	4.75	3.35	65.80	2.20	3.61	0.54	0.21	-	3.13
S	30.80	11.45	2.26	47.50	3.65	3.03	0.38	-	0.17	2.91
Pumice	75.1	12.5	2.00	0.425	0.072	0.018	5.67	0.086	3.55	1.35

Table 2. Properties of PE fibers

Material	Diameter (microns)	Length (mm)	Specific Gravity	Modulus of Elasticity (GPa)	Tenacity (GPa)	Color
PE Fibers	17.9	6,10	0.97	114	4.0	Off White

Table 3. Properties of MC as viscosity modifying admixture

Material	Viscosity (cP)	Degree of Substitution	Methoxy Substitution	Molecular Weight
MC	15	1.5-1.9	27.5-31.5	14,000

Mix Design

A control mixture was created using natural river sand (RS) as fine aggregates, with specified particle size, specific gravity, and water absorption capacity. Mineral admixture, such as ground granulated blast furnace Slag (S), was used to replace cement in mixtures. Two grades of pumice (Pumice 3 and Pumice 4) from CR Minerals New Mexico suppliers served as internal curing agent in the designed Engineered Cementitious Composite (ECC) for ambient

temperature environments. The chemical composition of the materials is provided in Table 1. Chemical composition of binders (C, S) and lightweight aggregate. The pumice was carefully blended to ensure optimal particle size distribution. The lightweight aggregates were presoaked into water for 24 hours and then added into the mix during mixing protocol. The mix design is outlined in Table 4.

Table 4. Mix proportions of ECC mixes (weight ratio to binder)

#	Mix ID	C/B	S/B	RS	Pumice	W/B	RS/B	MC (%)[1]	HRWR (%)[1]	PE Fibers (Vol%)[2]
1	S50-CT	0.5	0.5	1.0	0.0	0.31	0.313	0.01	0.0015	2.0
2	S50-P30	0.5	0.5	0.7	0.3	0.31	0.313	0.01	0.0015	2.0

Note: 1. HRWR and MC (% weight of the binder)
2. 1% of 6mm and 1% of 10mm PE Fibers (% of the total mix volume)

The mass of lightweight aggregates required for internal curing was calculated using the following equation (Dale P Bentz et al., 2011).

$$M_{LWA} = \frac{C_f \times CS \times \alpha_{max}}{S \times \emptyset_{LWA}}$$

Where:

M_{LWA} = mass of lightweight aggregates
C_f = binder content
CS = chemical shrinkage
α_{max} = degree of hydration
S = degree of saturation
Φ_{LWA} = Absorption

Equation 1. Mass of Lightweight Aggregates for Internal Curing

All mixtures included ADVA 195, a polycarboxylate-based high range water reducer (HRWR) compliant with ASTM C494, at a proportion of 0.0018% by weight of the total mix. Additionally, a viscosity-modifying admixture (MC), detailed in Table 3, was incorporated to tailor rheological properties and enhance printing quality. PE fibers were added to each mix at a volume of 2.0% to mitigate early age cracking in printed filaments. Mixing procedures shown in Figure 4 involved 10 minutes of dry blending followed by 5 minutes post-water addition for consistency. Subsequently, PE fibers were added, and mixing continued for 10 minutes: 5 minutes at a slow speed and 5 minutes at a medium speed to ensure uniform fiber dispersion.

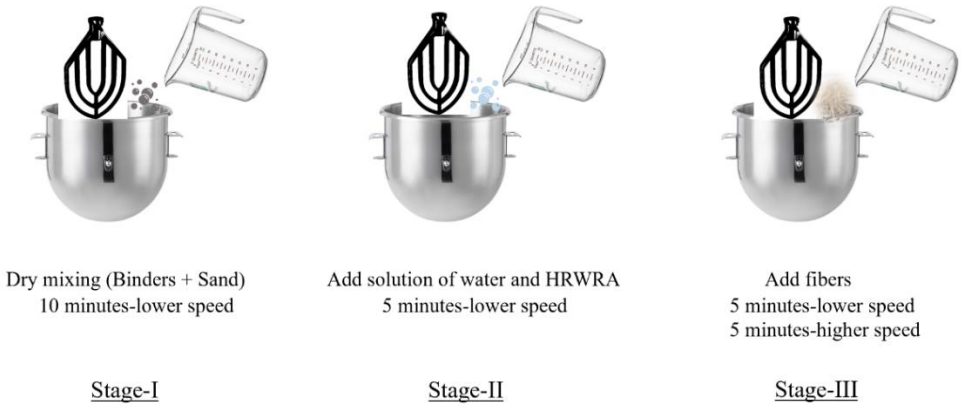

Figure 4. Mixing protocol for ECC Mixes

Test Methods

3D Printing System

A gantry 3D printer housed in the Dana C. Wood Materials and Structures Lab at the University of New Mexico shown in Figure 5 was used to evaluate the printability of the formulated mixes. This printer features a controller responsible for translating STL files into G-code which means converting a 3D model's mesh into machine instructions that tell a printer exactly how to move, extrude material, and build the object layer by layer and overseeing printing parameters such as speed, extrusion rate, and layer height. With three linear degrees of freedom, the printer's drive motors maneuver a 20mm diameter circular nozzle along X, Y, and Z axes. Print quality was evaluated based on extrudability and buildability.

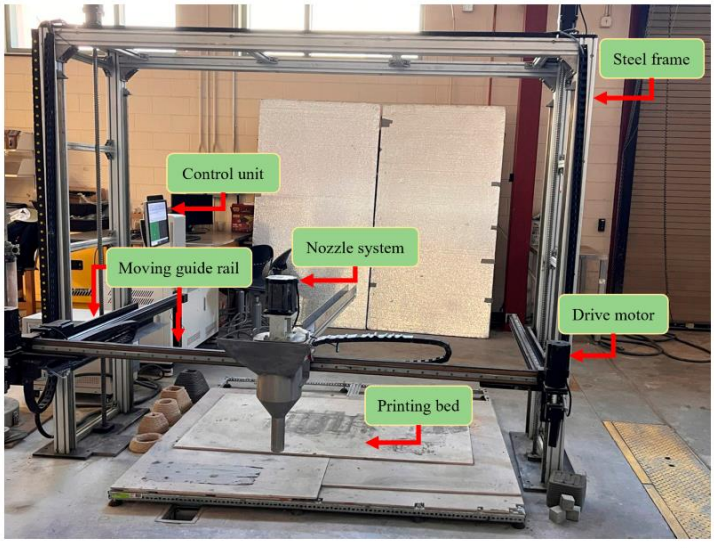

Figure 5. The 3D Gantry printing system in Dana C. Wood Materials and Structures Lab at the University of New Mexico

To examine the printability of the designed mixes based on their fresh properties, a series of experiments was performed to establish the relationship between the fresh properties and the printing performance of 3D printed elements. This included analyses of extrudability, shape retention, and buildability, all of which are detailed in this study.

Flow table test

The flow table test is shown in Figure 6. The flowability of the mix plays a crucial role in 3D printing of concrete as it governs the various stages of the printing process, such as pumping, extrudability, and buildability. Therefore, it was essential to adjust the flowability of the mix to make it printable. The quick preliminary flow test of mortars was performed following ASTM C1437–20 to determine the adequacy of the adjusted water content for each mix. To perform this test, the fresh mix was placed in the center of the flow table, filling half of the cone. The material as then tamped 20 times, followed by adding a second layer to fill the cone, tamping it as specified for the first layer. Excess material on the cone's surface was removed, and the cone was gently lifted. Subsequently, the flow table was dropped 25 times within 15 seconds, and the diameter of the specimens was measured at the end of the test. Finally, an average of three replicates was calculated for each mix.

Extrudability evaluation

The extrudability of various mixtures was evaluated by printing a zigzag pattern with six sides. Each mixture underwent extrusion rate calibration at speeds of 0.1, 0.15, and 0.20 rounds per second to ensure precise material deposition. Printing speeds ranging from 10 mm/sec to 35 mm/sec were tested on each side of the pattern to identify the optimal speed for consistent filament width. After 24 hours, filament width was measured at three sections to evaluate shape retention. Measurement consistency was analyzed to assess uniformity and reliability across mixtures and printing speeds.

Buildability evaluation:

Buildability was evaluated by printing a 20 mm x 400 mm wall to measure the maximum height each mixture can be printed before failure occurs.

Compressive Strength test

For the printed specimens created from each mixture, a primary prism sample consists of five layers in 243×200 mm and a total height of 50 mm printed using the gantry system. After 24 hours, the samples were moist cured in different regimes until the testing day. Cubes of 50×50×50mm were extracted from the primary printed sample using a wet tile saw during the testing day. All specimens were tested Normal to the printing direction. The cubes were tested after 28 days at a loading rate of 35 Psi according to ASTM C109-20. Compressive strength test setup is shown in Figure 7. Figure 8 displays the 3D-printed cubes prepared for the compressive strength tests.

Figure 6. Flow table test

Figure 7. Compressive strength test setup

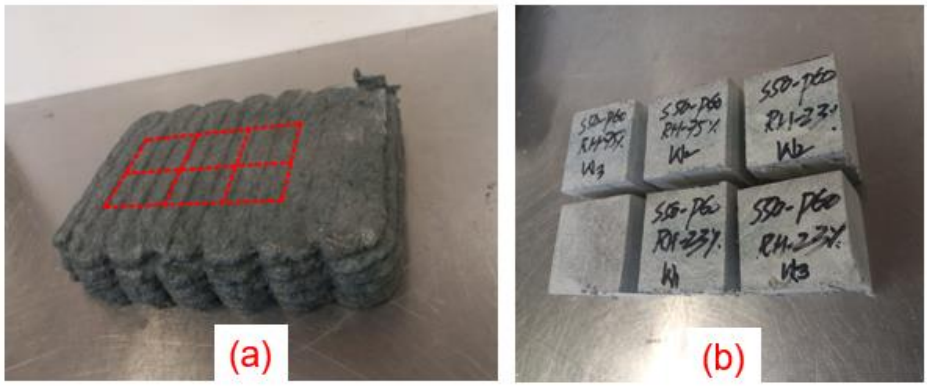

Figure 8. (a) Primary 3D printed slab of 243×200×50mm with 20 mm with circular nozzle (b) six extracted 50×50×50mm cubic samples from the primary sample

Flexural Strength Test

This research also evaluated the flexural behavior of ECC 3D-printed beams. Rectangular Primary specimens with 4 layers have been printed using the gantry system with the 20 mm diameter circular nozzle. The specimens were transferred to the different curing conditions till the testing day (28-days after printing). The printed beams were subjected to pure bending; a three-point flexural test has been conducted on the specimens using a hydraulic universal testing system. The load rate applied to the specimens was 0.00393 in/min. During the three-point bending test, the applied load was recorded on a recording systems software. The machine automatically recorded the displacement of the ECC specimens by LVDT's connected to the Universal testing machine. Figure 9 displays the testing machine and 3D-printed specimen.

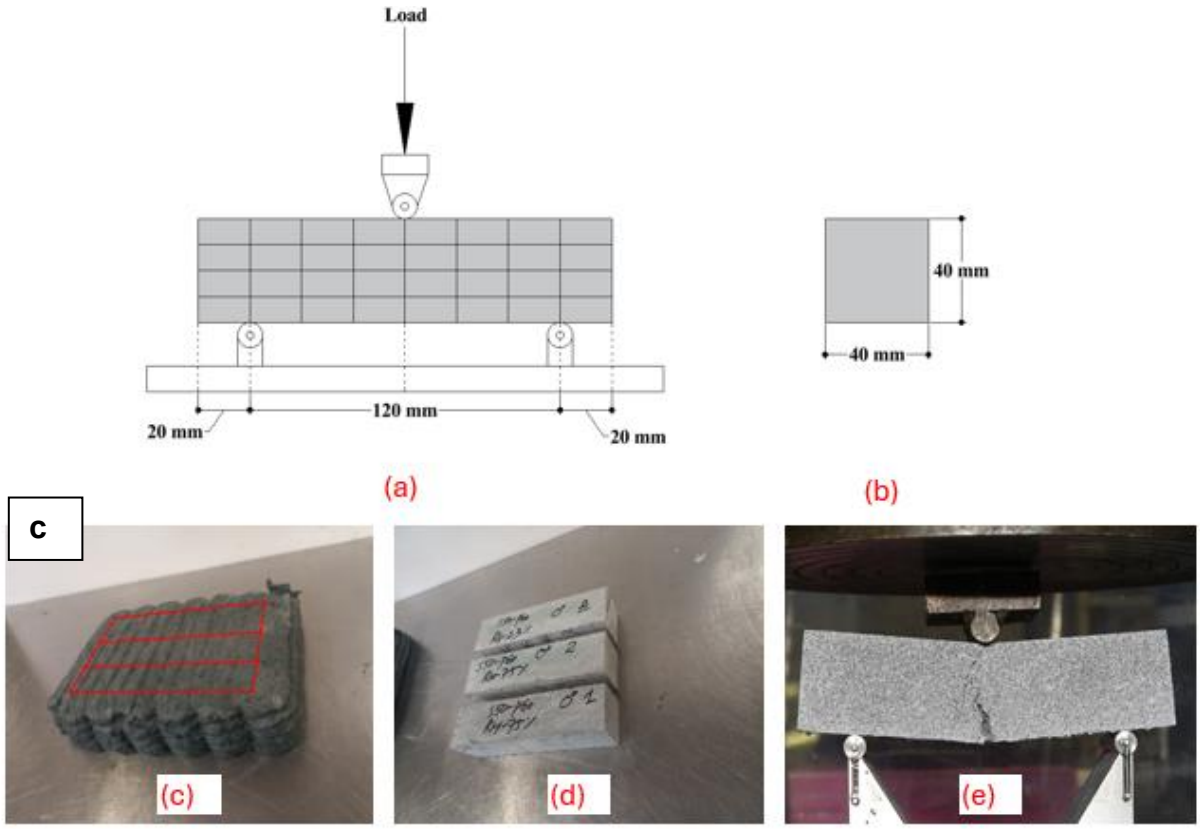

Figure 9. (a) Three point bending schematic test setup, (b) Cross section of tested beam, (c) Primary 3D printed slab of 243 x 200 x 50 mm with 20 mm circular nozzle (d) Three extracted prisms of 40 x40 x 160 mm, (e) Bending test setup

Chapter 4. Results and Discussions

Gradation, Surface Morphology and Microscopic Properties of Fine Aggregates

Error! Reference source not found. illustrates the particle size distribution of river sand (RS), pumice (P3 & P4) and their blends with pumice at two replacement levels, 30 % (P30) and 60 % (P60). The gradation of the fine aggregates was carried out using the standard test method for sieve analysis of fine aggregates conforming to ASTM C136/C136-19. Well-graded curves were observed for all the fine aggregates, showing a continuous distribution of particle sizes ranging from 0.1 mm to 2 mm. With a fineness modulus (FM) of 2.60 and an average particle size (d50) of around 0.7 mm, RS showed a smooth and continuous gradation curve, representing uniform particle packing. P3 with FM of 1.92 and an average particle size of 0.4 mm displayed a uniformly graded curve. In contrast, P4 had an FM of 2.87 with a d_{50} of 0.8 mm, showing a well-graded curve with all particle sizes. Additionally, P30 had FM of 2.60 with an average particle size of around 0.7 mm, and its gradation curve also overlapped the RS curve, representing a balanced particle size distribution conforming to similar packing density and enhanced internal friction in the composite. In contrast, P60 had a fineness modulus of 2.46, with an average particle size of 0.6 mm, representing fine gradation. Scanning electron microscopy (SEM) was carried out using JEOL 5800LV SEM furnished with the secondary and backscattered electron and cathodoluminescence (CL) imaging detectors located at the Institute of Meteoritics, University of New Mexico. Scanning electron microscopy was performed to characterize the morphology of fine aggregates, shown in **Error! Reference source not found.**, which revealed distinct differences; RS particles were angular with dense and smooth surface texture, resulting in stable particle interlocking. In contrast, pumice particles were highly porous with interconnected pores and vesicular microstructure. Internal curing is facilitated by this porous morphology of pumice, which affects the rheology and hydration of composites. The SEM images of these aggregates are presented in

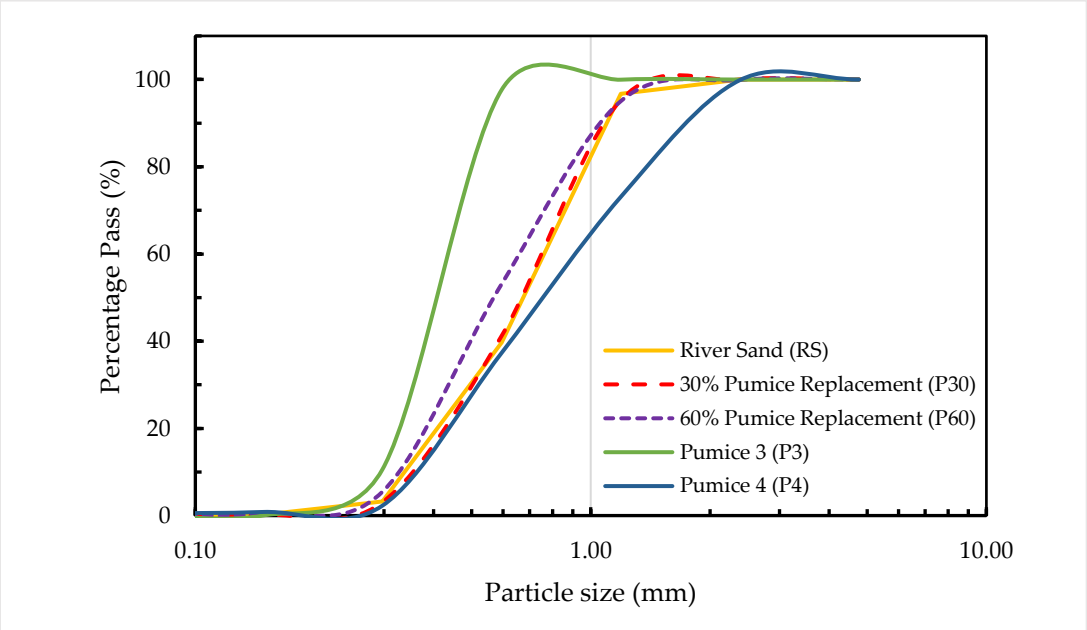

Figure 10.The gradation curves of the river sand (RS) and its blends with pumice.

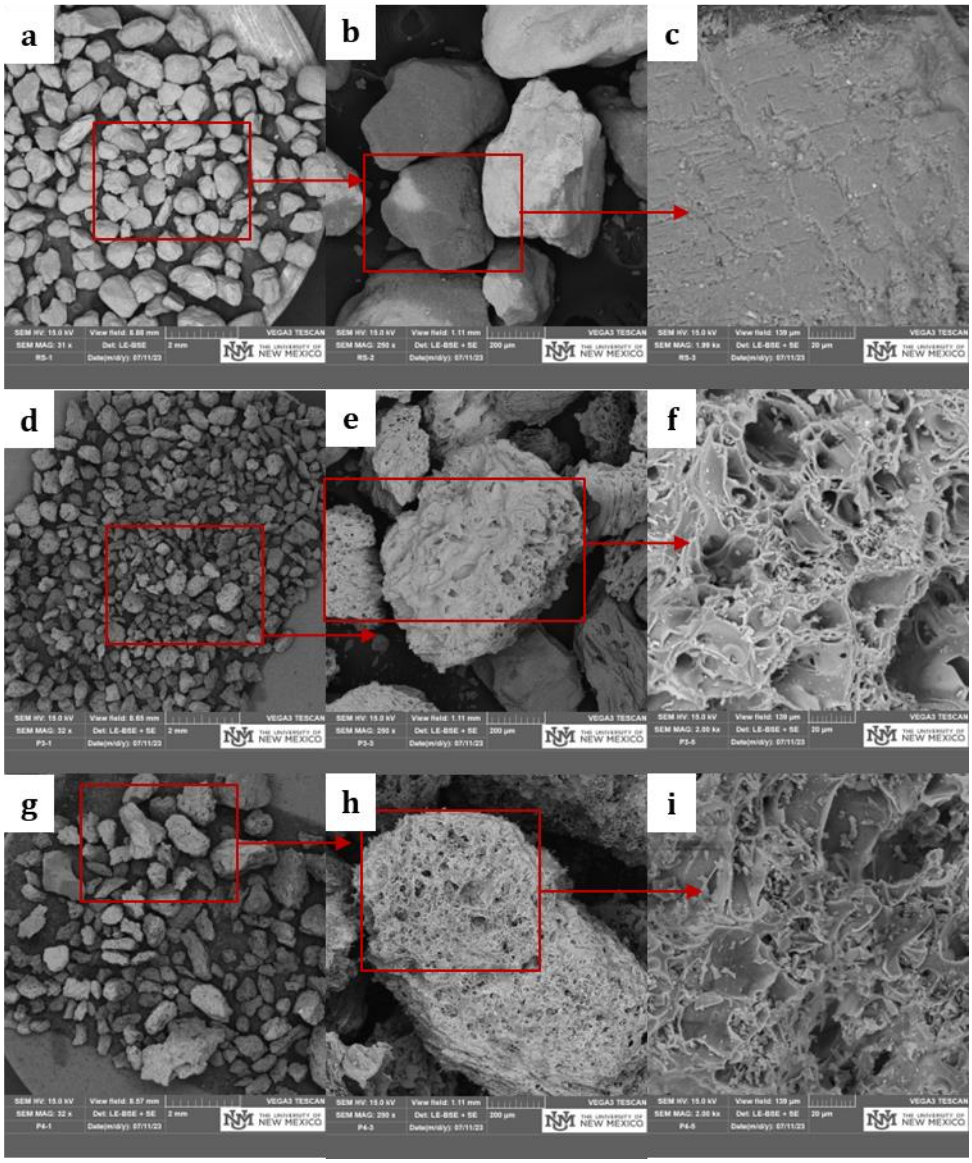

Figure 11.

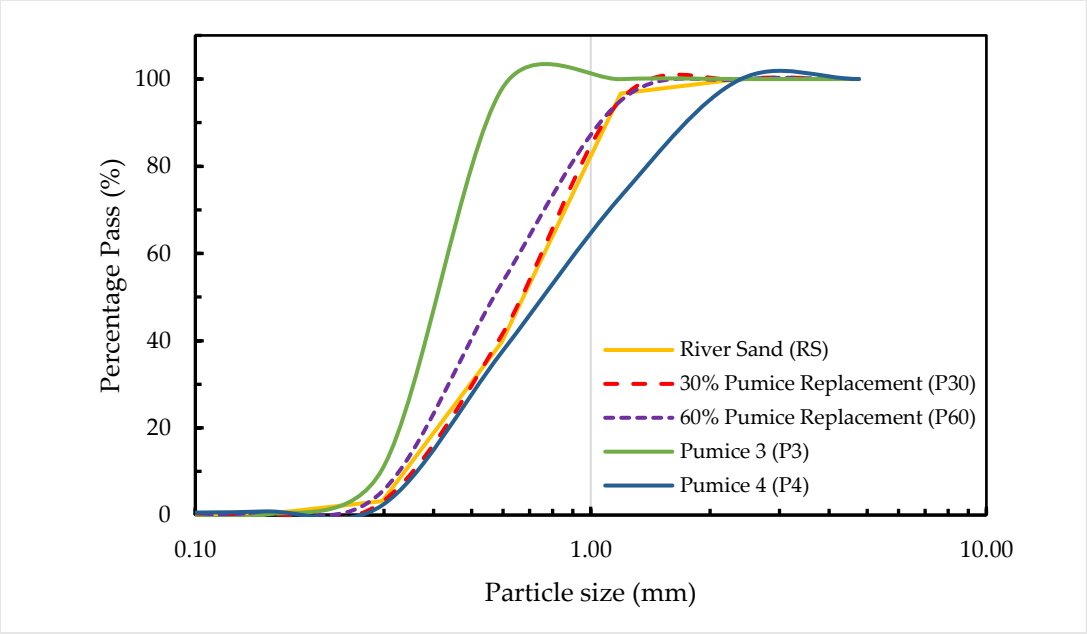

Figure 10.The gradation curves of the river sand (RS) and its blends with pumice.

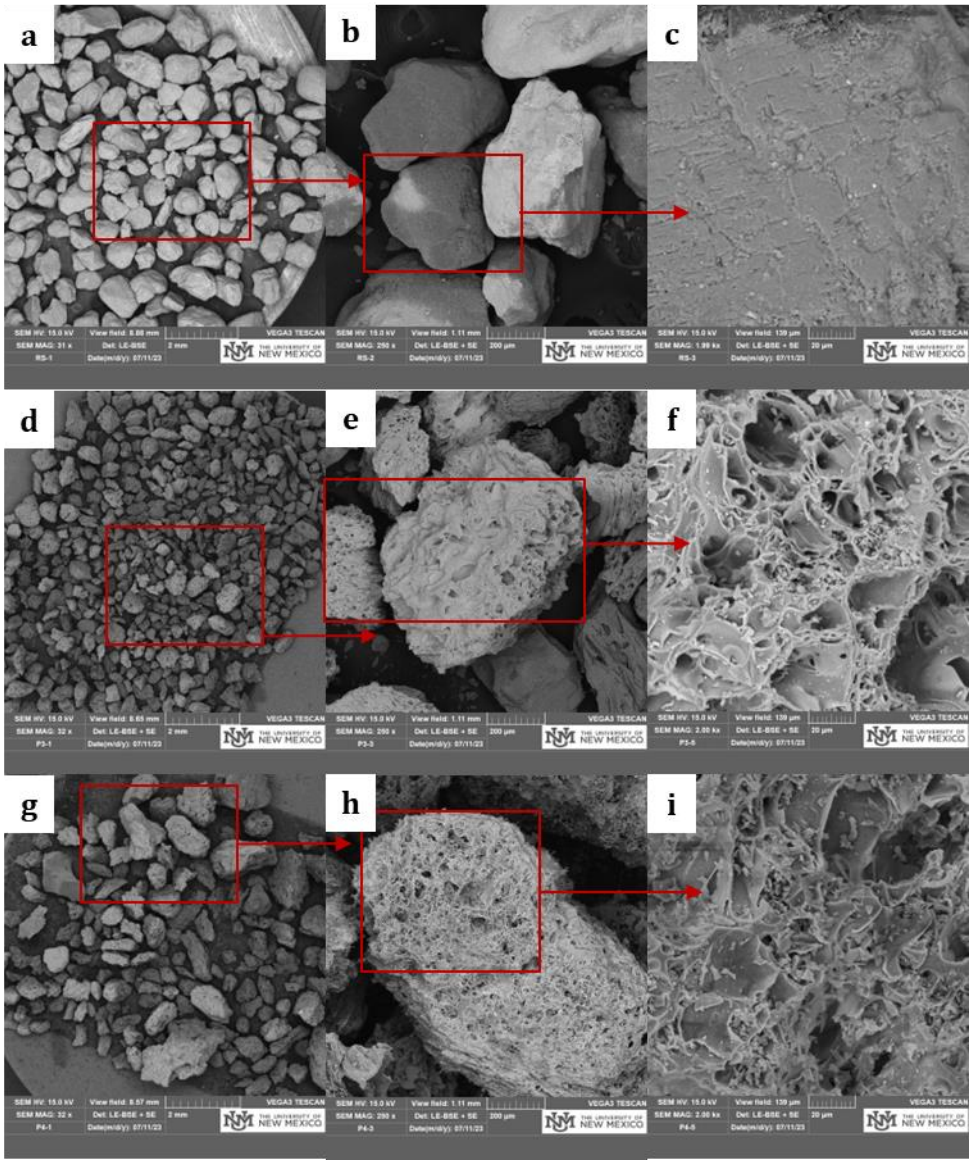

Figure 11. SEM micrographs of River sand (a, b, c), pumice 3 (d, e, f) and Pumice 4 (g, h, i) at different magnifications.

Flowability

The rheological properties and extrusion performance of 3D printed mixes depend on the mix's flowability. Figure 12 shows the flow table results for the S50-CT (control) and S50-P30 mixes, where the initial water-to-binder ratio was set at 0.27. Adjustments were made to this ratio to achieve flow diameters between 12 and 15 cm, as previous research from the PI's group indicated that this range is ideal for producing flowable, pumpable, and buildable mixes before testing for printing. Mixes with high fly ash content needed less water due to the lubricating effect of the fine, spherical fly ash particles, whereas slag-based mixes required more water. The inclusion of methylcellulose (MC) significantly altered the flow behavior, as previous studies recommended a flowability range of 16 to 20 cm for successful 3D concrete extrusion. Despite achieving a flow diameter in the range of 12 to 14.25 cm with MC, the mix apparently looks

good for extrudability at high rates, which is in contrast with conventional concrete mixes without MC. This discrepancy is likely due to the water retention properties of cellulose ethers in ECC mixes, which prevent water migration between pores. Additionally, the stickiness of the mix when in contact with the flow table surface can hinder its flow, and MC can cause the agglomeration of cement particles and hydration products, increasing dynamic yield stress and plastic viscosity, thus reducing flowability. While the flow table test provides initial insights into the necessary water content for printing mixes, it is a subjective measure that should be complemented with rheological assessments and preliminary printing tests for a comprehensive evaluation. In the next step of this study, the water content will be further adjusted for the actual printing tests and according to the rheological properties of fresh mixes.

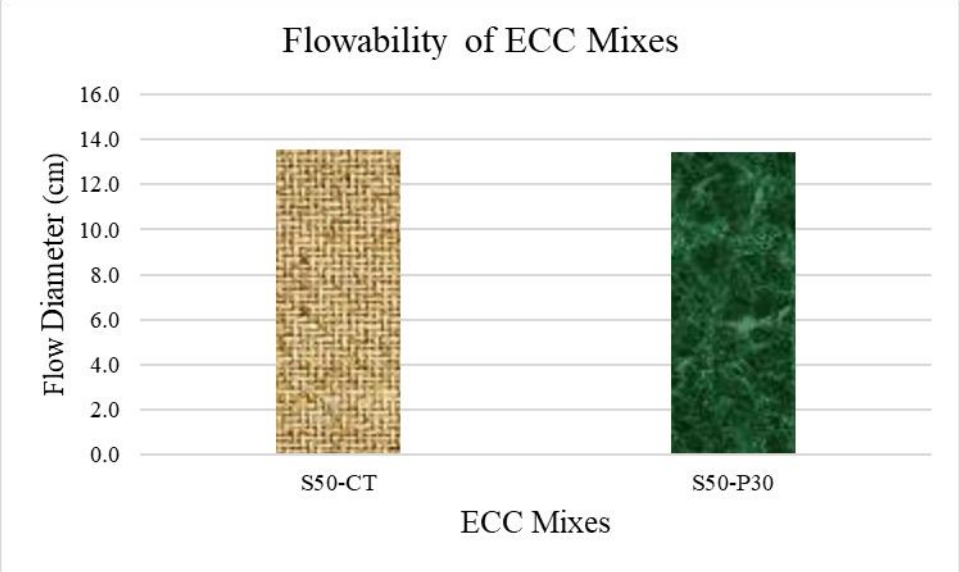

Figure 12. Flowability of ECC Mixes

Extrudability

In this study, extrudability refers to the capability of the 3D printing process to produce components that meet satisfactory standards in terms of dimensions, consistency, and surface quality of the printed filaments. It evaluates the overall quality and performance of the printed objects by examining their dimensional accuracy, uniformity, and surface finish. To assess the extrudability of the designed mixes, a zigzag path was printed at various speeds. Before conducting the extrudability test, the extrusion rate was calibrated for the mix. Once a consistent rate was established, the mixes were evaluated at a constant extrusion speed. The printing speed was incrementally increased from 10 mm/s to 35 mm/s along each side of the zigzag pattern, as shown in Figure 13, to determine the optimal speed for each mix. The width of the printing path was measured immediately after completing the zigzag pattern to select the printing speed that resulted in the least deviation from the design. Furthermore, to ensure the dimensional conformity of each mix, after 24 hours, final measurements were made on hardened printed filaments width. The printed filament width of S50-CT was found to be 23.6mm and the printing speed and extrusion rate were 10mm/sec and 0.10 rounds per sec respectively. For S50-P30 the filament width was 24.0 mm whereas the printing speed was 10 mm/sec, and the extrusion rate was 0.10 rounds per sec. These printed filament widths are close to the intended design width of 20 mm (diameter of the nozzle) and confirms the dimensional consistency.

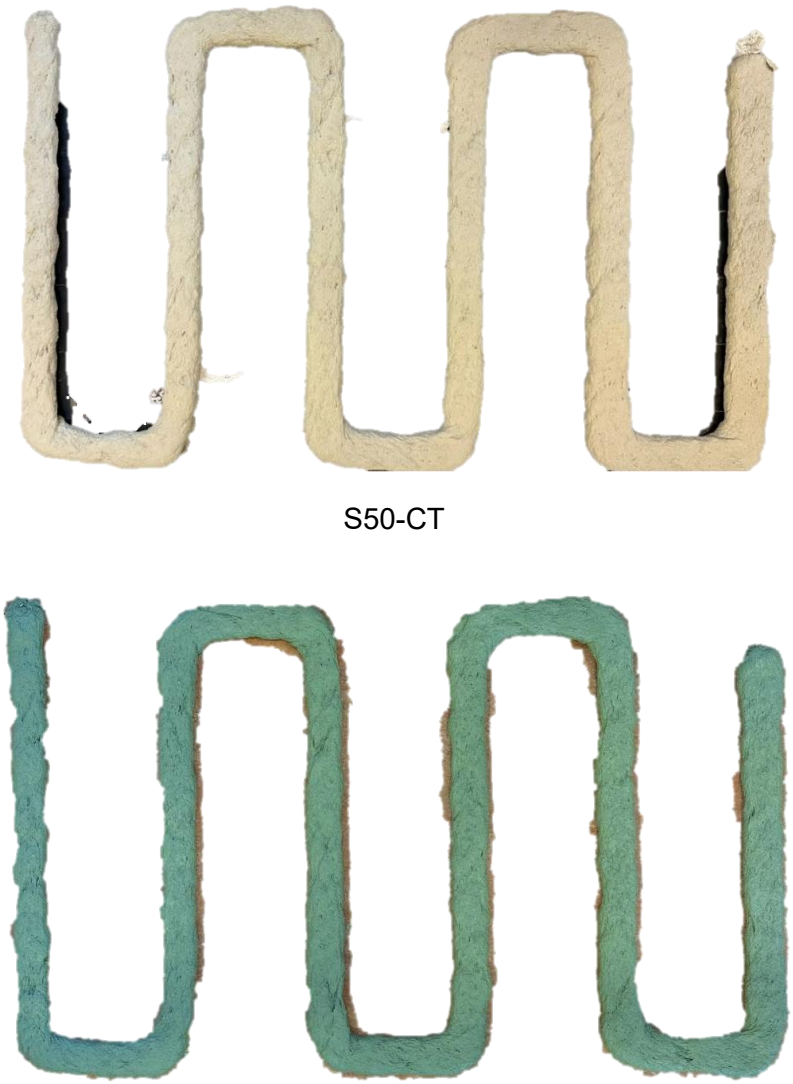

S50-CT

S50-P30

Figure 13. Extrudability on zigzag printing path for fresh and hardened states of S50-CT, and S50-P30

Buildability

In concrete 3D printing, buildability also known as structural buildup, is referred to the ability of the printed filaments or layers to withstand the self-weight and the weight of the subsequent layers without any possible failure in the fresh state. This failure can be due to the deformation in the bottom layer, or it can be a buckling failure, depending upon the location of the failure. It can also be because of the self-weight of the layer, weight of the following layers and extrusion pressure of the nozzle. Shape stability and buildability are the key objectives and play a vital role in the evaluation of design mixes for printability. Generally, the shape stability and

buildability are closely associated to the rheology of the mix, particularly the static yield stress plays an important role in structural buildup. For evaluation of the buildability a 20mm X 400mm wall was printed. Before printing the wall extrudability of the mix was checked on the zigzag pattern and optimum printing parameters were determined. Buildability evaluation of the mixes S50-CT and S50-P30 are presented in Figure 14. For S50-CT the printing speed and extrusion were kept constant at 10mm/sec and 0.10 rounds/sec and a maximum of 18 layers were printed before failure. For S50-P30 the printing speed was 10mm/sec and extrusion was kept constant at 0.10 rounds/sec and the maximum number of layers printed was 16.

S50-CT

S50-P30

Figure 14. Buildability evaluation of the mixes S50-CT and S50-P30

Compressive Strength

The 28-day compressive strength of ECC mixes is presented in Figure 15. The printed specimens were subjected to three different curing conditions till the age of 28 days, (a) moist curing room with RH-100% and 24±0.5°C (b) sealed chamber with sodium chloride saturated salt solution with RH-75% and 24±0.5°C (c) lab environment with RH-18% and 24±0.5°C. Both S50-CT and S50-P30 exhibit the highest compressive strength under 100% RH. This highlights the beneficial effects of internal curing at saturated conditions, ensuring full hydration and better

microstructural development. Compressive strength slightly decreases compared to RH-100% for both mixes. This suggests that partial humidity reduces hydration efficiency, but the reduction is not drastic, indicating that the mixes retain some ability to sustain hydration. The compressive strength is significantly lower for the S50-CT mix at RH-18%, with a notable drop and higher variability (indicated by larger error bars). Interestingly, the S50-P30 mix shows better performance under RH-18% compared to S50-CT, with a smaller reduction in strength. This implies that S50-P30 may have enhanced internal curing mechanisms or greater moisture retention capacity, which mitigates strength loss under dry conditions. S50-P30 Performance: The superior performance of S50-P30 at low RH may be attributed to its composition, potentially containing materials (e.g., pre-saturated lightweight aggregates or polymers) that provide internal water reservoirs for hydration. S50-CT Limitations: the significant drop in strength for S50-CT at RH-18% indicates its dependency on external moisture for curing, making it less suited for dry environments. When designing ECC for environments with low humidity, incorporating internal curing agents like those in S50-P30 can be crucial to maintaining mechanical properties. The compressive strength was in the range of 7.5 to 10.2 Ksi with a minimum of 7.5 Ksi at RH-18% and a maximum of 10.2 Ksi at RH-100%. The two mixes exhibited lower strength with low humidity, but the internally cured mix (S50-P30) did not undergo significant changes with variations in RH, which is a sign that the mix retained more moisture and was less susceptible to drying.

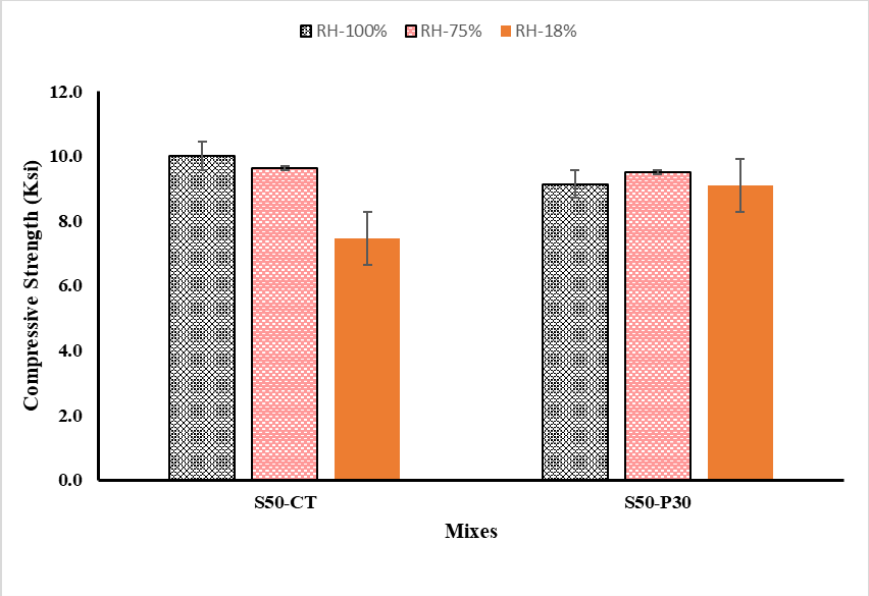

Figure 15. Compressive Strength test results

Flexural Strength

The flexural ultimate load (average of 3 samples) capacities and corresponding displacements (average of 3 samples) are shown in Figure 16 and 17. The 28-day flexural load-displacement behavior of ECC mixes, S50-CT and S50-P30 is presented in Figure 188-Figure 22. The printed specimens were subjected to three different curing conditions till the age of 28 days, (a) moist curing room with RH-100% and 24±0.5°C (b) sealed chamber with sodium chloride saturated

salt solution with RH-75% and 24±0.5°C (c) lab environment with RH-18% and 24±0.5°C. A similar initial linear elastic phase can be observed from the graphs, where load changes were proportional to displacement. This illustrates the uncracked behavior of the mixes. S50-CT (RH-100%) and S50-P30 (RH-75%) both reach a similar peak load, so their maximum flexural strengths are comparable. Therefore, both mixes can be inferred as bearing similar magnitudes of flexural loading before significant amounts of cracking occur. S50-CT, after hitting its peak, there is an abrupt drop in load followed by small peaks and valleys. This type of pattern indicates sudden cracking events and poor crack-bridging capacity. The load rapidly reduces with displacement, suggesting brittle failure and limited ductility.

In S50-P30, the post-peak load drops more gradually and exhibits a smoother curve compared to S50-CT. This indicates better crack-bridging and energy absorption capacity. Flexural behavior suggests higher ductility and a more stable failure process. In terms of displacement, S50-P30 sustains larger displacements compared to S50-CT before failure. This highlights its improved toughness and ability to withstand deformation. In S50-CT, the brittle failure and sharp load drops indicate that the control mix lacks internal curing mechanisms, leading to insufficient hydration under non-saturated conditions. Without internal curing agents, the mix is more prone to cracking and less capable of maintaining integrity after peak load. S50-P30, the smoother post-peak curve and better displacement capacity are indicative of enhanced internal curing mechanisms, likely due to the inclusion of water-retaining agents. Internal curing promotes better hydration, resulting in improved microstructural bonding and crack-bridging capacity. The maximum load of 651 lbs. was recorded for S50-P30 whereas minimum load of 454 lbs. for the control mix S50-CT at RH-100%. Similarly, the maximum displacement of 0.22 inch was observed for S50-P30 at RH-75% and minimum displacement of 0.12 inch was observed for S50-CT at RH-100%. The findings indicate that load capacity and displacement of the ECC mixes were affected by the relative humidity with some degree of significance. In control mix (S50-CT) the load capacity went up to fully saturated conditions to 75 percent RH followed by slight decline at 18 percent RH, which implied that moderate drying enhanced better matrix consolidation and severe drying initiated degradation of strength. The internally cured mixture (S50-P30) had a greater load capacity than the control at all humidity levels and at its best under saturated conditions indicating the advantage of internal moisture retention that pumice provides. The same trend was applied in displacement, and both mixes exhibited the greatest deformation at 75 percent RH. S50-P30 mix always demonstrated higher displacement as compared to the control, which proved higher ductility owing to internal curing. The differences in performance of 18 percent RH when using both mixes indicate how sensitive ECC is to over drying and the improved behavior of S50-P30 under all environments indicate its greater ability to withstand changes in moisture.

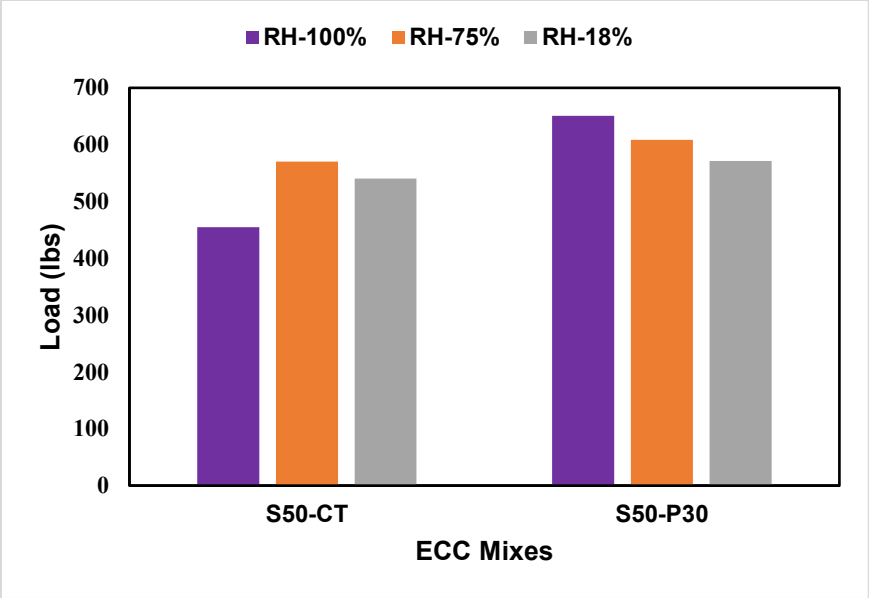

Figure 16. Flexural Load Capacities (Average) for ECC Mixes

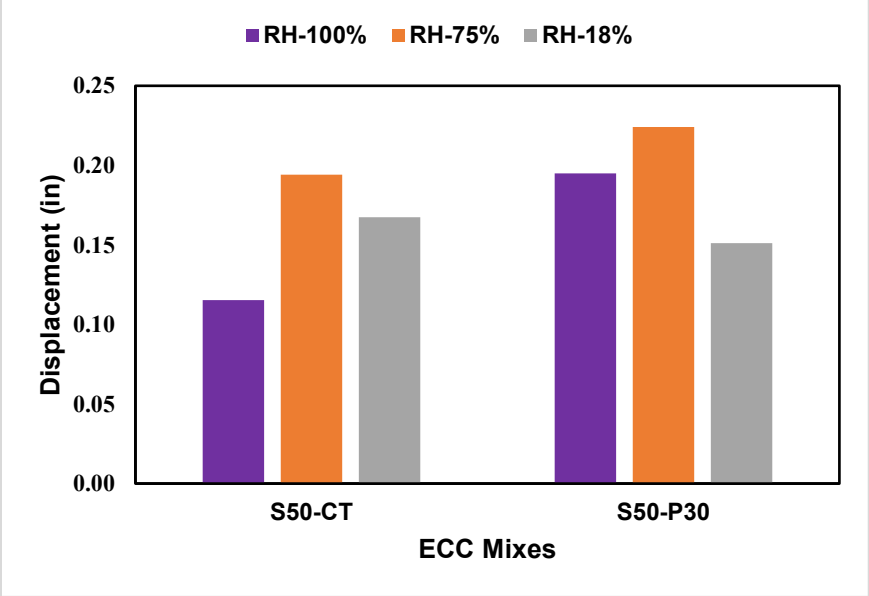

Figure 17. Mid Span Displacements (Average) for ECC Mixes at Ultimate Average Loads

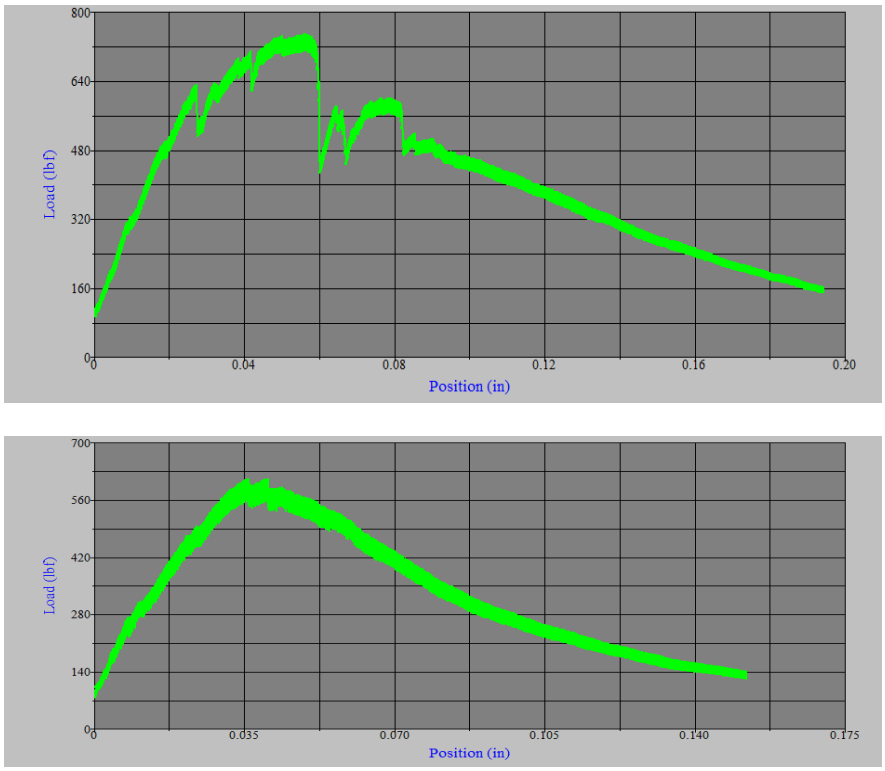

Figure 18. Load vs. Displacement curves of S50-CT at RH-100%

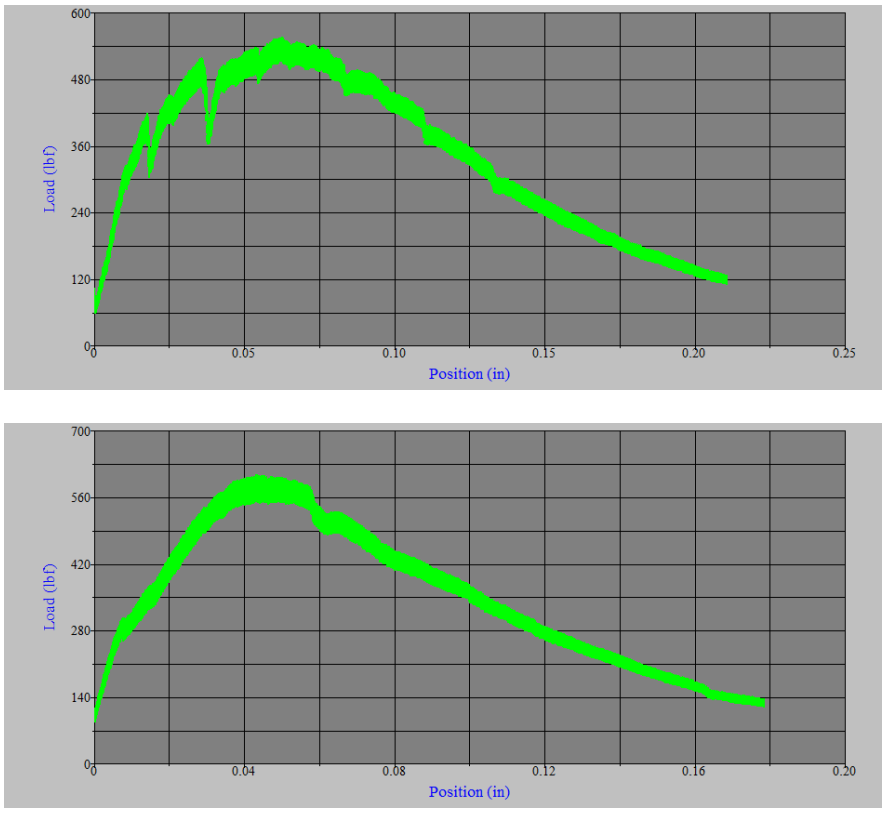

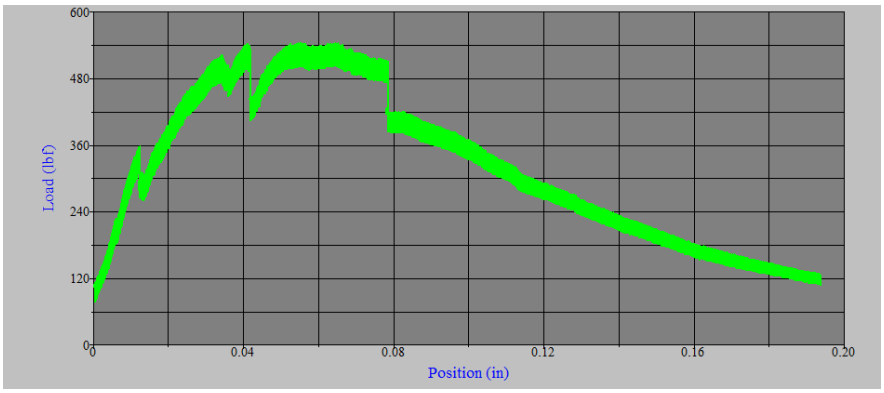

Figure 19. Load vs. Displacement curves of S50-CT at RH-75%

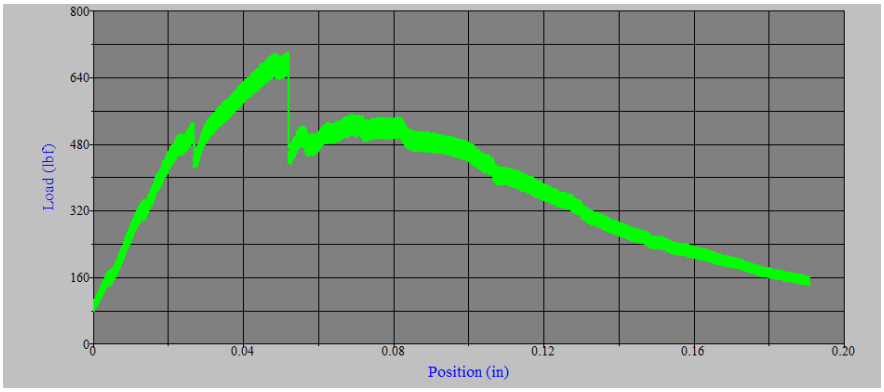

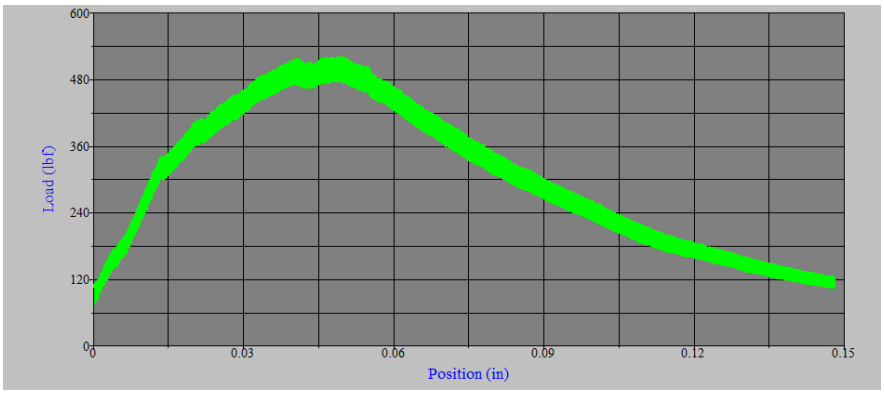

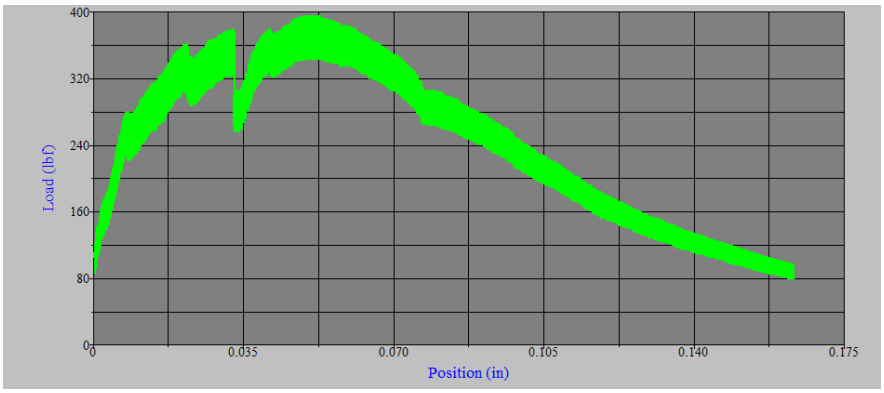

Figure 20. Load vs. Displacement curves of S50-CT at RH-18%

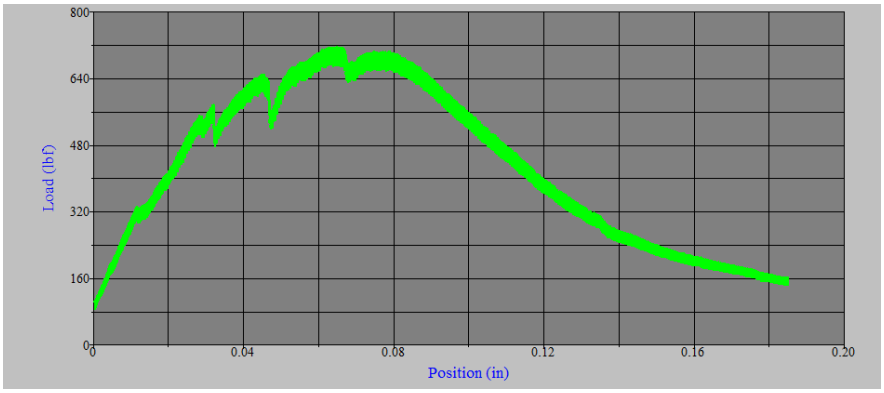

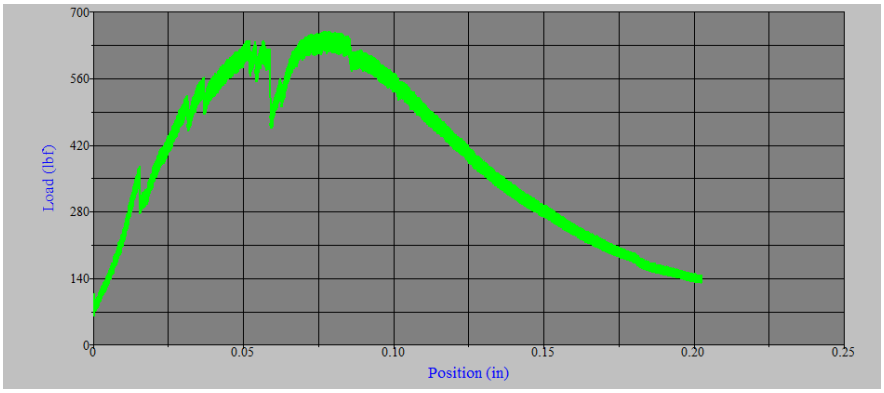

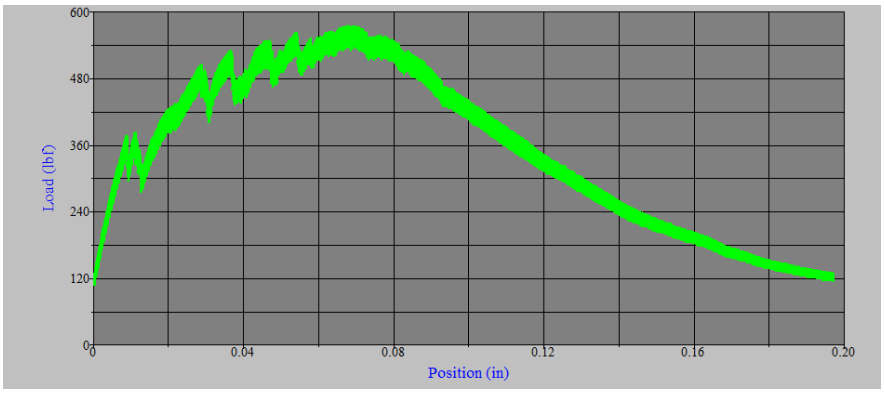

Figure 21. Load vs. Displacement curves of S50-P30 at RH-100%

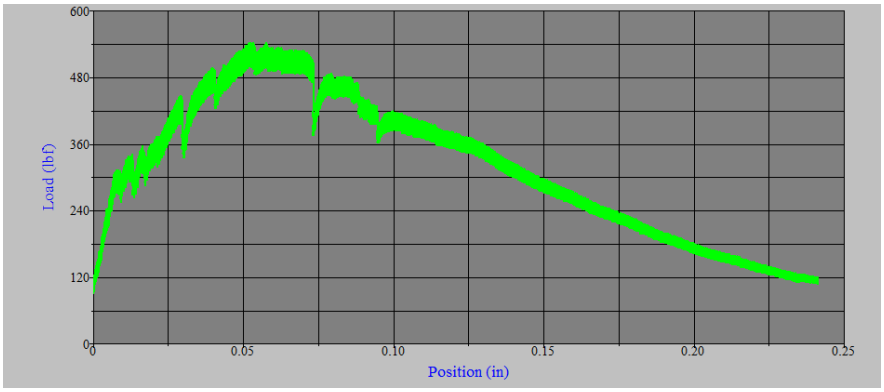

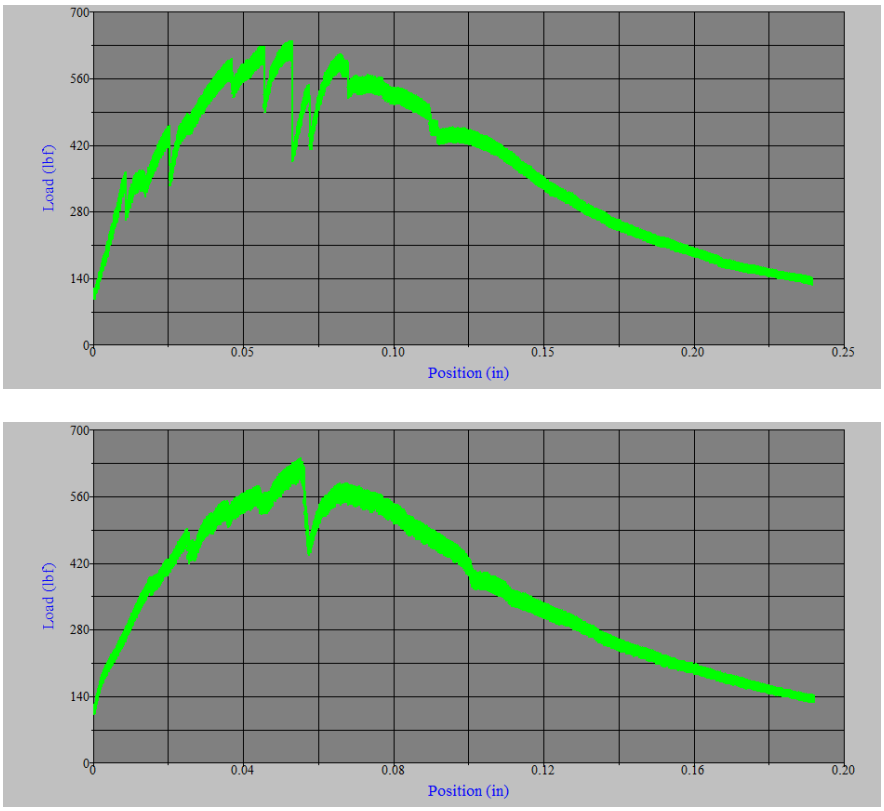

Figure 22. Load vs. Displacement curves of S50-P30 at RH-75%

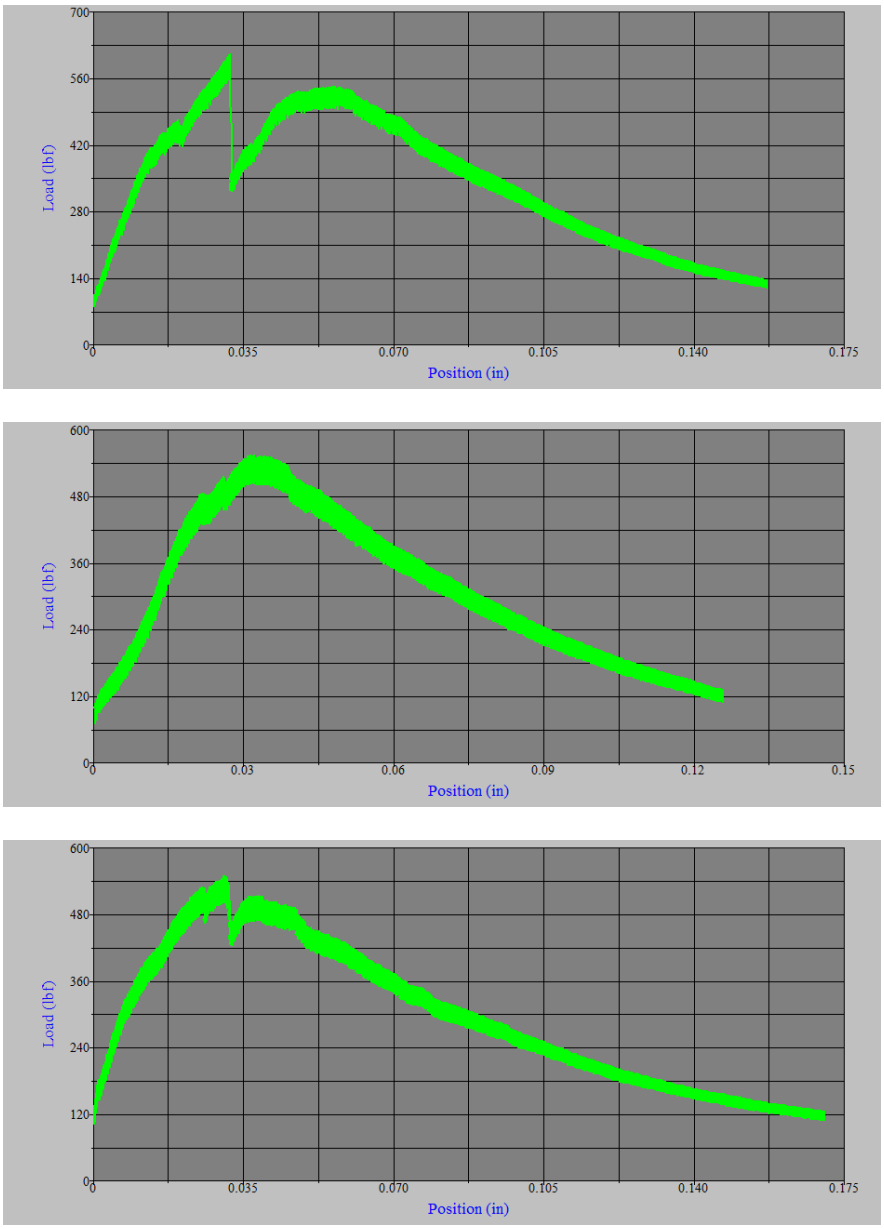

Figure 23.Load vs. Displacement curves of S50-P30 at RH-18%

In conclusion, S50-P30 demonstrates superior flexural toughness, ductility, and energy absorption compared to S50-CT, making it a more suitable choice for environments requiring durable and crack-resistant materials. The role of internal curing in S50-P30 is evident from its enhanced post-peak performance, which reduces the risk of sudden failure.

Chapter 5. Conclusions and Recommendations

This research aimed to advance the application of 3D printing by using self-reinforced ECC mixes in transportation projects, contributing to deployable and durable solutions in southern regions. ECC's unique properties, such as enhanced durability and crack resistance, can lead to longer-lasting structures with reduced need for frequent repairs and replacements. This longevity directly translates to lower material consumption in production. Moreover, ECC often incorporates supplementary cementitious materials like fly ash and slag, which are byproducts of industrial processes and can replace a portion of cement in the mixture. This substitution not only improves material performance but also can reduce the cost of the concrete. ECC's high ductility also allows for thinner sections and reduced material volumes, further minimizing time and energy related to production and transportation. This study aimed to investigate whether internal curing can enhance the curing process of 3D printed ECC components in arid environments, particularly in regions like the southwest United States, where prolonged dry conditions exist.

1. The inclusion of presoaked pumice LWAs slightly reduced the flowability of S50-P30 mix as compared to S50-CT mix which could be attributed to the coarser texture and particle angularity resulting in increased inter-particle friction.
2. The extrudability test was performed to evaluate the printing quality of the ECC mixes with and without lightweight aggregates. It revealed that incorporation of PE fibers at a volume of 2% reduced the printing quality but it increased the crack resistance. Incorporation of PE fibers also increased the shape retention capability of the filaments; therefore, the width of the printed filaments was close to the designed width.
3. The buildability test results indicated that the control mix S50-CT had higher number of stacked layers as compared to S50-P30. This can be attributed to the reduced internal water content into the mix as compared to S50-P30 mix. As S50-P30 mix contains presoaked pumice lightweight aggregates which release water with the passage of time and increase the water content which effects the buildability.
4. Both the mixes, S50-CT and S50-P30 showed reduction in compressive strength with the decrease in relative humidity, which underscores the effect of environmental conditions on the curing and hydration.
5. At low relative humidity (RH-18%), S50-P30 illustrated improved performance as compared to S50-CT, which suggests the effectiveness of internal curing mechanisms in S50-P30 under harsh environmental conditions, mitigating the moisture loss and ensuring continued hydration.
6. The compressive strength of S50-P30 (RH-75%) is equivalent to S50-CT (RH-100%) and even higher than S50-P30 (RH-100%), which also ensures the effectiveness of internal curing.
7. In terms of flexural strength, S50-CT and S50-P30 both showed comparable peak loads, demonstrating similar initial flexural capacity, whereas S50-CT shows a brittle post peak behavior with sudden load drop and limited energy dissipation. In contrast, S50-P30 shows a more gradual post peak reduction, indicating higher ductility, toughness and crack bridging capabilities.
8. In terms of displacements, S50-P30 sustains larger displacements as compared to S50-CT which indicates improved resistance to deformations and enhanced durability in flexure.

In conclusion, the improved performance of S50-P30 underscores the effectiveness of internal curing mechanisms, which ensures continuous hydration and enhances the microstructural integrity of the ECC mixes and improves the crack resistance, especially under harsh environmental conditions. Whereas S50-CT lacks these mechanisms, resulting in reduced performance.

Chapter 6. Implementation of Project Outputs

This study aimed to investigate the development of 3D printable cementitious mixes optimized for constructing infrastructure using the internal curing approach to enhance their properties. As a result, the project output will produce experimental results, images, and documentation files, including the final report. The outcomes of this research endeavor encompass a range of valuable outputs. These include exploring and potentially developing internal curing methods for optimizing 3D printable cementitious mixes tailored to infrastructure construction. Through this investigation, the study yielded experimental findings, visual documentation in the form of images, and comprehensive documentation files. These outputs contribute to a better understanding of enhancing material properties through internal curing techniques.

Impacts/Benefits of Implementation

The outcome of this research project could potentially bring changes and improvements to the transportation system. These improvements in material performance can lead to several positive impacts on the transportation system. The outcomes of this research project encompass a multifaceted approach aimed at advancing transportation infrastructure in low-humid regions. These outcomes/impacts include:

1. **Innovative Manufacturing Techniques:** Implement cutting-edge 3D printing methods for transportation infrastructure projects specifically tailored for regions with low humidity. Explore and adapt emerging technologies to suit the unique construction needs of these areas.
2. **Optimized 3D Printable Cementitious Mixes:** Develop and fine-tune cementitious mixes suitable for 3D printing, with a focus on incorporating internal curing agents. Extensive testing and optimization are conducted to ensure these mixes meet the project's mechanical and durability requirements.
3. **Improved Material Performance:** Enhance the mechanical and durability performance of infrastructure components by utilizing the optimized 3D printable cementitious mixes. Evaluate and validate these improvements through rigorous testing protocols.
4. **Longevity and Durability Enhancement:** Utilize internal curing agents in ECC mixes to promote better hydration and crack resistance. This will extend the lifespan of constructed infrastructure elements, reducing the need for frequent repairs and maintenance.
5. **Cost Reduction Strategies:** Explore cost-effective construction methodologies by leveraging 3D printing and ECC mixes. Investigate the potential for eliminating traditional formwork and reducing labor demands. Maximize the use of locally available resources to further minimize construction costs.
6. **Enhanced Structural Integrity:** Ensure that 3D-printed ECC elements exhibit superior mechanical properties, leading to stronger and more reliable transportation structures. Prioritize the safety and well being of commuters and travelers by creating robust infrastructure components.
7. **Environmental Resilience**: Improve the resilience of infrastructure components, making them more reliable under various environmental conditions. This will contribute to a more dependable transportation system for users.
8. **Educational and Workforce Development:** Foster educational and workforce development opportunities by engaging graduate students and offering research roles to undergraduates. This initiative helps train a skilled and knowledgeable workforce for the transportation sector.

Chapter 7. Technology Transfer and Community Engagement and Participation (CEP) Activities

The research findings will be disseminated and shared with stakeholders interested in the study outcomes through presenting at conferences or publishing technical papers. The research project places importance on transferring its technological findings or innovations to practical use. These efforts will contribute to making the transportation sector more robust and capable of withstanding challenges while also being more able to endure over time.

Chapter 8. Invention Disclosures and Patents, Publications, Presentations, Reports, Project Website, and Social Media Listings

The findings of this study will be incorporated into several courses taught by the PI, including her materials course at UNM and the seminar course for graduate students.

Publications, Presentations, Reports, Project Website, and Social Media Listings
Currently, no publications stemming from this research, but the findings will be published soon in a high-rank journal in construction materials.

Invention Disclosures and Patents
As of now, there are no invention disclosures or patents stemming from this research.

References

ASTM Committee F42 on Additive Manufacturing Technologies. (2009).

Bentz, D. P., & Snyder, K. A. (1999). Protected paste volume in concrete: Extension to internal curing using saturated lightweight fine aggregate. *Cement and Concrete Research*, *29*(11), 1863–1867. doi: 10.1016/S0008-8846(99)00178-7

Bentz, Dale P, & Weiss, W. J. (2011). *Internal curing : A 2010 State-of-the Art Review*. Gaithersburg, MD. doi: 10.6028/NIST.IR.7765

Biyani, Y., Patil, L. G., & Kurhe, C. N. (2020). Engineered Cementitious Composites. In Learning and Analytics in Intelligent Systems (Vol. 2). doi: 10.1007/978-3-030-24314-2_27

Chen, Y., Jansen, K., Zhang, H., Romero Rodriguez, C., Gan, Y., Çopuroğlu, O., & Schlangen, E. (2020). Effect of printing parameters on interlayer bond strength of 3D printed limestone-calcined clay-based cementitious materials: An experimental and numerical study. *Construction and Building Materials*, *262*, 120094. doi: 10.1016/J.CONBUILDMAT.2020.120094

Jason Weiss, Dale Bentz, Anton Schindler, P. L. (2012). Internal Curing-Constructing More Robust Concrete. *Structure*, *January*, 10–14.

Kim, H. K., & Lee, H. K. (2018). Hydration kinetics of high-strength concrete with untreated coal bottom ash for internal curing. *Cement and Concrete Composites*, *91*(January), 67–75. doi: 10.1016/j.cemconcomp.2018.04.017

Kim, J. H., Choi, S. W., Lee, K. M., & Choi, Y. C. (2018). Influence of internal curing on the pore size distribution of high strength concrete. *Construction and Building Materials*, *192*, 50–57. doi: 10.1016/J.CONBUILDMAT.2018.10.130

Kong, H.-J., Bike, S., & Li, V. (2003). Constitutive Rheological Control to Develop a Self-Consolidating Engineered Cementitious Composite Reinforced with Hydrophilic Polyvinyl alcohol Fibers. *Cement and Concrete Composites*, *25*, 333–341. doi: 10.1016/S0958-9465(02)00056-2

Li, V. C. (2003). On Engineered Cementitious Composites (ECC). *Journal of Advanced Concrete Technology*, *1*(3), 215–230. doi: 10.3151/jact.1.215

Li, V. C., Bos, F. P., Yu, K., McGee, W., Ng, T. Y., Figueiredo, S. C., Nefs, K., Mechtcherine, V., Nerella, V. N., Pan, J., van Zijl, G. P. A. G., & Kruger, P. J. (2020). On the emergence of 3D printable Engineered, Strain Hardening Cementitious Composites (ECC/SHCC). *Cement and Concrete Research*, *132*(March), 106038. doi: 10.1016/j.cemconres.2020.106038

Liu, J., Shi, C., Ma, X., Khayat, K. H., Zhang, J., & Wang, D. (2017). An overview on the effect of internal curing on shrinkage of high performance cement-based materials. *Construction and Building Materials*, *146*, 702–712. doi: 10.1016/J.CONBUILDMAT.2017.04.154

Ma, L., Zhang, Q., Jia, Z., Liu, C., Deng, Z., & Zhang, Y. (2022). Effect of drying environment on mechanical properties, internal RH and pore structure of 3D printed concrete. *Construction and Building Materials*, *315*(July 2021), 125731. doi: 10.1016/j.conbuildmat.2021.125731

Mechtcherine, V., Gorges, M., Schroefl, C., Assmann, A., Brameshuber, W., Ribeiro, B., Cusson, D., Custódio, J., Silva, E., Ichimiya, K., Igarashi, S., Klemm, A., Kovler, K., Lopes, A., Lura, P., Nguyen, V., Reinhardt, H.-W., Toledo Filho, R., Weiss, W., & Zhutovsky, S. (2013). Effect of internal curing by using superabsorbent polymers (SAP) on autogenous shrinkage and other properties of a high-performance fine-grained concrete: Results of a RILEM round-robin test. *Materials and Structures/Materiaux et Constructions*, 1–22. doi: 10.1617/s11527-013-0078-5

Moelich, G. M., Kruger, P. J., & Combrinck, R. (2022). Mitigating early age cracking in 3D printed concrete using fibres, superabsorbent polymers, shrinkage reducing admixtures, B-CSA cement and curing measures. *Cement and Concrete Research*, *159*(June), 106862. doi: 10.1016/j.cemconres.2022.106862

Moelich, Gerrit M., Kruger, J., & Combrinck, R. (2020). Plastic shrinkage cracking in 3D printed concrete. *Composites Part B: Engineering*, *200*, 108313. doi: 10.1016/J.COMPOSITESB.2020.108313

Moelich, Gerrit Marius, Kruger, J., & Combrinck, R. (2021). Modelling the interlayer bond strength of 3D printed concrete with surface moisture. *Cement and Concrete Research*, *150*, 106559. doi: 10.1016/J.CEMCONRES.2021.106559

Nerella, V. N., Hempel, S., & Mechtcherine, V. (2019). Effects of layer-interface properties on mechanical performance of concrete elements produced by extrusion-based 3D-printing. *Construction and Building Materials*, *205*, 586–601. doi: 10.1016/J.CONBUILDMAT.2019.01.235

Robayo-Salazar, R., Mejía de Gutiérrez, R., Villaquirán-Caicedo, M. A., & Delvasto Arjona, S. (2023). 3D printing with cementitious materials: Challenges and opportunities for the construction sector. *Automation in Construction*, *146*(September 2022). doi: 10.1016/j.autcon.2022.104693

Şahmaran, M., Lachemi, M., Hossain, K. M. A., & Li, V. C. (2009). Internal curing of engineered cementitious composites for prevention of early age autogenous shrinkage cracking. *Cement and Concrete Research*, *39*(10), 893–901. doi: 10.1016/j.cemconres.2009.07.006

Sanjayan, J. G., Nematollahi, B., Xia, M., & Marchment, T. (2018). Effect of surface moisture on inter-layer strength of 3D printed concrete. *Construction and Building Materials*, *172*, 468–475. doi: 10.1016/J.CONBUILDMAT.2018.03.232

Schroefl, C., Snoeck, D., & Mechtcherine, V. (2017). A review of characterisation methods for superabsorbent polymer (SAP) samples to be used in cement-based construction materials: report of the RILEM TC 260-RSC. *Materials and Structures*, *50*. doi: 10.1617/s11527-017-1060-4

Sedghi, R., Zafar, M. S., & Hojati, M. (2023). Exploring Fresh and Hardened Properties of Sustainable 3D-Printed Lightweight Cementitious Mixtures. *Sustainability (Switzerland)*, *15*(19). doi: 10.3390/su151914425

Soja, W., Georget, F., Maraghechi, H., & Scrivener, K. (2020). Evolution of microstructural changes in cement paste during environmental drying. *Cement and Concrete Research*, *134*, 106093. doi: 10.1016/J.CEMCONRES.2020.106093

Van Der Putten, J., Snoeck, D., De Coensel, R., De Schutter, G., & Van Tittelboom, K. (2021). Early age shrinkage phenomena of 3D printed cementitious materials with superabsorbent polymers. *Journal of Building Engineering*, *35*, 102059. doi: 10.1016/J.JOBE.2020.102059

Wang, L., Tian, Z., Ma, G., & Zhang, M. (2020). Interlayer bonding improvement of 3D printed concrete with polymer modified mortar: Experiments and molecular dynamics studies. *Cement and Concrete Composites*, *110*, 103571. doi: 10.1016/J.CEMCONCOMP.2020.103571

Yang, J., Sun, Z., De Belie, N., & Snoeck, D. (2024). Internal curing and its application to alkali-activated materials: A literature review. *Cement and Concrete Composites*, *145*(November 2023), 105360. doi: 10.1016/j.cemconcomp.2023.105360

Yang, L., Shi, C., Liu, J., & Wu, Z. (2021). Factors affecting the effectiveness of internal curing: A review. *Construction and Building Materials*, *267*, 121017. doi: 10.1016/j.conbuildmat.2020.121017

Zafar, M. S., Bakhshi, A., & Hojati, M. (2023a). Printability and shape fidelity evaluation of self-reinforced engineered cementitious composites. *Construction and Building Materials*, *408*(October), 133676. doi: 10.1016/j.conbuildmat.2023.133676

Zafar, M. S., Bakhshi, A., & Hojati, M. (2023b). Printability and shape fidelity evaluation of self-reinforced engineered cementitious composites. *Construction and Building Materials*, *408*(October), 133676. doi: 10.1016/j.conbuildmat.2023.133676

Zhutovsky, S., Kovler, K., & Bentur, A. (2002). Efficiency of lightweight aggregates for internal curing of high strength concrete to eliminate autogenous shrinkage. *Materials and Structures/Materiaux et Constructions*, *34*(246), 97–101. doi: 10.1007/bf02482108

Zhutovsky, Semion, Kovler, K., & Bentur, A. (2004). Influence of cement paste matrix properties on the autogenous curing of high-performance concrete. *Cement and Concrete Composites*, *26*(5), 499–507. doi: 10.1016/S0958-9465(03)00082-9

Appendix A: Technical Parameters of 3D-Printer

Cartesian Coordinate 3D-Printer Technical Parameters

Technical parameters of JYHC 3D printing gantry robot system (3DPRT)		
Frame structure	Size: length (mm) * width (mm) * height (mm)	2800*2010*2600
Frame structure	Weight (Kg)	300
Frame structure	Drive motor	Stepper motor, five
Frame structure	Power supply	AC 220V
Mixing and feeding system	Shear mixer Capacity (L) Voltage (V) Power (W) Weight (Kg)	 50 (recommended) (max 60) 380 AC 3000 300x2
Mixing and feeding system	Pumping system Voltage (V) Power (W) Horizontal transmission distance (M) Transmission height (m) Weight (Kg)	 380 AC 4000 15 5 180
Mixing and feeding system	Transporting pipe: Material Length (m) Inner diameter (mm)	 Rubber 5 45
Motion control system	Effective size: length (mm) * width (mm) * height (mm)	1800*1600*1800
	XY Plane moving speed (mm/S)	10 to 350
	Z moving speed (mm/S)	10 to 20
Printing head	Diameter of printing head (mm)	25, 35, 45 mm
Printing head	The diameter of Acrylic printing head (mm)	40 mm
Printing head	Ways of adding material	Manual (through the printing head) or automatic (pumping system)
Software	Software development environment	LabVIEW (reads from a G-Code)
Software	Interface text	English
Software	Software upgrade	Network transmission, Free for renew

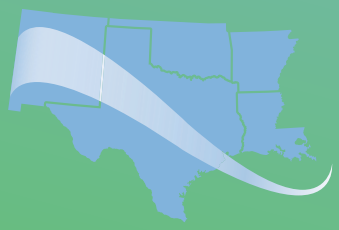

SOUTHERN PLAINS
TRANSPORTATION CENTER

The University of Oklahoma | OU Gallogly College of Engineering
202 W Boyd St, Room 213A, Norman, OK 73019 | (405) 325-4682 | Email: sptc@ou.edu